Detrital Zircon U-Pb Age Constraints on the Sandstone Provenance of the Upper Cretaceous Eutaw Formation from Central Alabama to Western Georgia

by

Michael A. Barrett

A thesis submitted to the Graduate Faculty of
Auburn University
in partial fulfillment of the
requirements for the Degree of
Master of Science

Auburn, Alabama
May 2, 2020

Eutaw Formation, Sandstone Provenance, Tombigbee Sand Member, Detrital Zircon

Approved by

Dr. Haibo Zou, Chair, Professor, Department of Geosciences
Dr. David King, Professor, Department of Geosciences
Dr. Ashraf Uddin, Professor, Department of Geosciences

ABSTRACT

Sandstone provenance analysis of the Tombigbee Sand Member and Eutaw Formation is vital to discerning source material of clastic detrital sediments found in eastern Alabama and western Georgia along the Upper Cretaceous coastal plain boundary. Geochemical methods and grain-size analysis give insight into the relationship between Upper Cretaceous coastal plain boundary clastic sediment accumulations and potential erosional sources. Utilizing detrital zircon grains in U-Pb radiometric dating, detrital zircon age populations were analyzed to determine erosional sources of the Eutaw Formation. Their overall zircon age distributions are dominated by Grenvillian zircons (44-46%) followed by Taconian zircons (23-33%) with minor Acadian and Alleghanian zircons. Their age distributions are similar to the detrital zircon age distributions of Appalachian rivers suggesting their origin from the Appalachian mountain. The lack of zircon age peaks at greater than 1.8 Ga indicates that Ouachitas were not a significant source for the sandstones in this study. Geochemical and grain-size analysis revealed a well-sorted, quartz dominated sediment composition included in the Eutaw Formation suggesting increased sediment transport and possible chemical weathering. The results of this study suggest greater sediment influx from older upper-continental sources from the Appalachian Mountains, transported by the Chattahoochee River system. Provenance investigation through geochemical and grain-size analysis of the Eutaw Formation has helped to further constrain our depositional understanding of eastern Alabama and western Georgia along the Upper Cretaceous coastal plain outcrop belt.

ACKNOWLEDGMENTS

There are many people who have been invaluable to the progression and completion of both this research and my graduate education here at Auburn University. I'd like to thank my parents for their support of my education and career pursuits. Special thanks to my fiancé, Katie, for cheering me on and providing encouraging words on rough days. I want to thank Sandor Ricketts and Pedro Montalvo-Jimenez on their insight into provenance and discussion of my data. I would also like to thank my office mates for the laughs, beers, and collaboration throughout these years. Thank you to my advisor, Dr. Haibo Zou, for his guidance and support throughout this project along with an introduction into the world of sandstone provenance. Thanks for all your guidance; this project would not have progressed without you! Funding and resources for this research were provided by the American Chemical Society Petroleum Research Fund (PRF# 57500-UR2) won by Dr. Haibo Zou and Dr. David King Jr and by the Radiogenic Isotope Lab at Auburn University. The ion microprobe facility at UCLA is partly supported by a grant from the Instrumentation and Facilities Program, Division of Earth Sciences, National Science Foundation. Dr. Ming-Chang Liu from UCLA provided assistance with ion probe analysis. Special Thanks to Dr. Ashraf Uddin for his belief in me throughout this project and for serving on my thesis committee along with Dr. David King Jr. Dr. Zeki Billor has been a vital resource to my education in preparing and interpreting geochemical data. Dr. Charles Savrda gave guidance on sampling in Columbus, Georgia. Thank you to the staff of Auburn University for both training and help in using many of their instruments. And lastly, thank you to the Auburn University Department of Geosciences for providing me with the resources and support to pursue and continue my education!

TABLE OF CONTENTS

LIST OF FIGURES

LIST OF TABLES AND EQUATIONS

INTRODUCTION

1. 1 Research Purpose

1.1.1 Research Goal

This thesis aims to contribute to the understanding of sandstone provenance within the Upper Cretaceous Gulf Coastal Plain, specifically the Eutaw Formation in eastern Alabama and western Georgia from a sedimentological, geochronological, and geochemical perspective.

1.1.2 Research Objectives

The Upper Cretaceous Eutaw Formation of the Gulf Coast Plain of Alabama and western Georgia contains two stratigraphic sub-units: the upper Tombigbee Sand Member and an unnamed lower member. The Eutaw Formation is a light-greenish-gray to yellowish-gray cross-bedded, well-sorted, micaceous, fine to medium quartz sand that is fossiliferous and glauconitic in part and contains beds of greenish-gray micaceous, silty clay and medium-dark-gray carbonaceous clay (Szabo et al., 1988). The formation is known to include the accessory mineral, zircon (Barineau et al., 2015). The Gulf Coastal Plain Boundary extends from eastern Mississippi to western Georgia expanding over 300 miles (Figure 1). The depositional history of the Gulf Coastal Plain Boundary has been studied extensively due to its relevance to regional stratigraphy (e.g. Britton, 1968; Mancini and Tew, 1993; Osborne 2013), although little work has been done to understand the sandstone provenance of the Eutaw Formation in eastern Alabama and western Georgia.

Determining the source of the clastic sediment within the Eutaw Formation has implications for understanding the spatial and temporal distribution of clastic sediment

accumulation across eastern Alabama and western Georgia, and could aid in understanding clastic sediment distribution at other potential accumulation sites along the Gulf Coastal Plain Boundary. Clastic sediment accumulation is heavily influenced by eastern United States orogenic events and associated erosional periods (Holland and Patzkowsky, 1997). Changes in source lithology associated with orogenic events can alter clastic sediment flux volumes. In addition, distance from the shoreline and fluctuations in water depth can also control the distribution of clastic sediment deposition along the Gulf Coastal Plain Boundary.

The Eutaw Formation provides an excellent opportunity to explore the relationship between Upper Cretaceous coastal plain boundary clastic sediment accumulations and potential erosional sources. The objective of this research is to establish the provenance of clastic detritus in the Upper Cretaceous Eutaw Formation of eastern Alabama and western Georgia along the Upper Cretaceous Coastal Boundary.

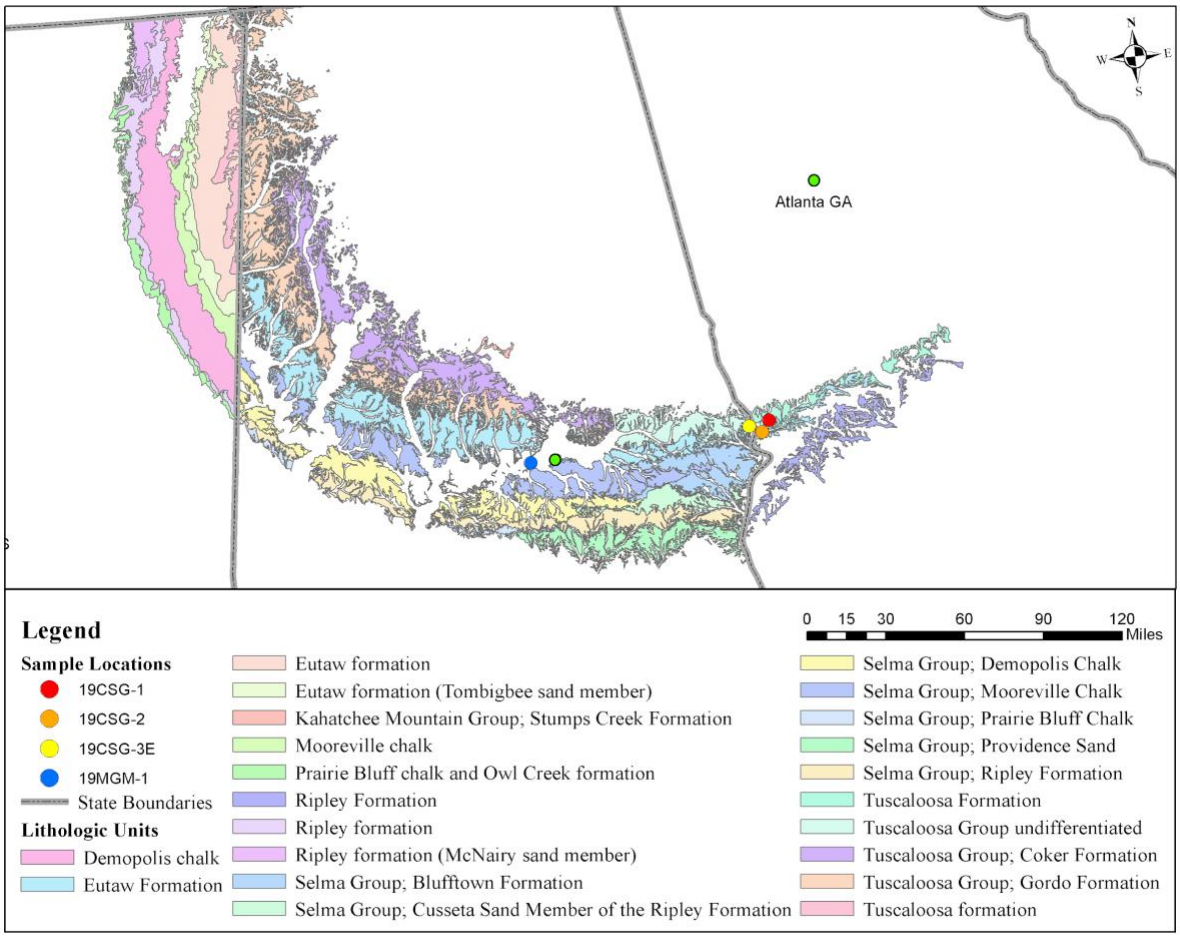

Figure 1. Regional geologic map of Upper Cretaceous formations in Alabama, Georgia, and Mississippi

1.2 Geologic Background

1.2.1 Tectonic Setting

The Eutaw Formation is part of the Gulf Coastal Plain, an area of Mesozoic and Cenozoic sediments that occupies the southern part of the state and extends into eastern Mississippi as well as western Georgia. In Alabama, the Gulf Coastal Plain forms a sweeping curve from Phenix City, in Russell County, to the Alabama-Mississippi border west of Florence, in Lauderdale County (Tew and Ebersole, 2008). In eastern Alabama, the northern boundary of the coastal plain makes contact with the Piedmont Upland and continues northeast into Georgia (Figure 2). Development of the Coastal plain is relatively young (~140 Ma to the present) and dominated by sedimentary rocks and sediment (Jones, 1967). Geologic units in the region are commonly composed of sediments being described as gravels, sands, silts, and clays. Sedimentary rocks associated with the Gulf Coastal Plain include rock variations composed of sandstones, limestone, claystone, and chalk.

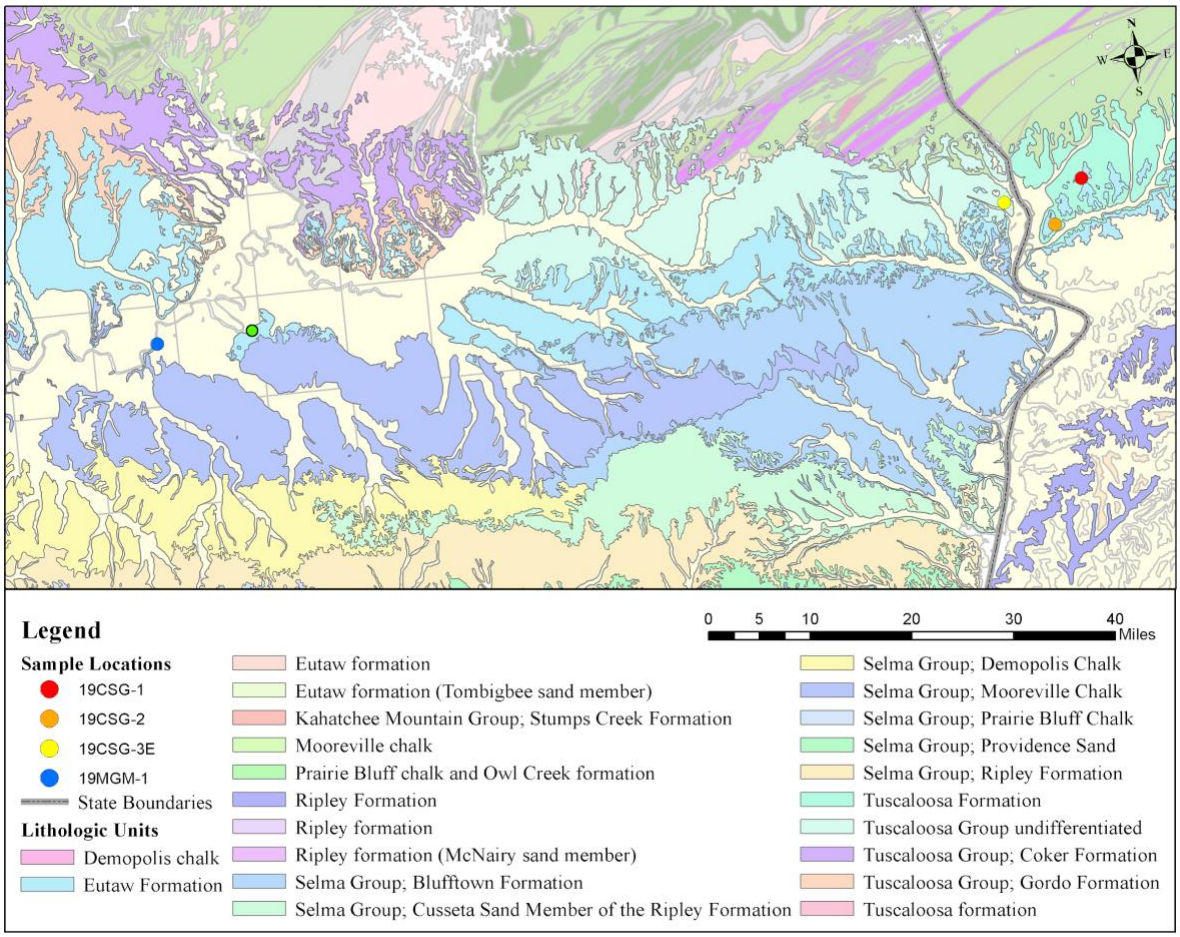

Figure 2. Geologic map of central and eastern Alabama featuring study area and the northern contact with the Piedmont Upland.

1.2.2 Stratigraphy of the Gulf Coastal Plain

Upper Cretaceous fine to medium-grained sediments within the Gulf Coastal Plain varies in nomenclature and expression across the southeastern United States. Nomenclature for associated units varies throughout the region but will be referred to in the context of the focus area interpretation.

The Eutaw Formation is a stratigraphic unit that can be found in Alabama, Georgia, and Mississippi. The Eutaw Formation continues eastward across Alabama eventually overlying the

Tuscaloosa Group near the Alabama River (Szabo et al., 1988). This formation is a light-greenish-gray to yellowish-gray cross-bedded, well-sorted, micaceous, fine to medium quartz sand that is fossiliferous and glauconitic in part and contains beds of greenish-gray micaceous, silty clay and medium-dark-gray carbonaceous clay (Szabo et al., 1988). The formation varies greatly from western Alabama to eastern Alabama with light-gray glauconitic fossiliferous sand, thin beds of sandstone, and massive accumulations of fossil oyster shells occurring locally in the upper part of the formation in western Alabama (Tombigbee Sand Member) and thin to thick-bedded accumulations of fossil oyster *Ostrea cretacea* Morton occurs throughout much of the formation in eastern Alabama (Szabo et al., 1988).

Although the Eutaw Formation is the focus of this study, similar lithostratigraphic units observed in the rock record will be utilized to create spatial consistency between sample locations. In Alabama, the Upper Cretaceous Eutaw Formation overlies the non-marine Tuscaloosa Group. The nomenclature for the Tuscaloosa Group differs between states with the unit being recognized as the Tuscaloosa Group in Alabama and the Tuscaloosa Formation in Georgia (Reinhardt et al., 1994). The poorly sorted sands of the Tuscaloosa range in grain size from fine to coarse sand. In eastern and central Alabama, the thickness of the Tuscaloosa can range from eight to eighty meters. Provenance studies have indicated fluvial and subaerial deltaic environments as possible depositional sources (Sayers and Uddin, 2010).

The Upper Cretaceous Eutaw Formation underlies the Selma Group. The Selma Group consists chiefly of sand, gravel, clay, and chalk (Copeland, 1968). In central Alabama, the Selma Group is composed of several formations including, in ascending order, the Mooreville Chalk, Demopolis Chalk, Ripley Formation, and Prairie Bluff Chalk. The Mooreville Chalk is in disconformable contact with the Tombigbee Sand Member, which is highlighted by a bed of

glauconitic, chalky sand containing phosphate pellets and molds of fossils (Russell and Keady, 1990). The Mooreville Chalk is a yellowish-gray to olive-gray compact fossiliferous clayey chalk and chalky marl (Szabo et al., 1988). The formation is known to be fossiliferous including mosasaur and dinosaur remains (Dobie, 1978). The Selma Group completes the Cretaceous system in Alabama with upper Santonian to Maastrichtian age strata (Figure 3).

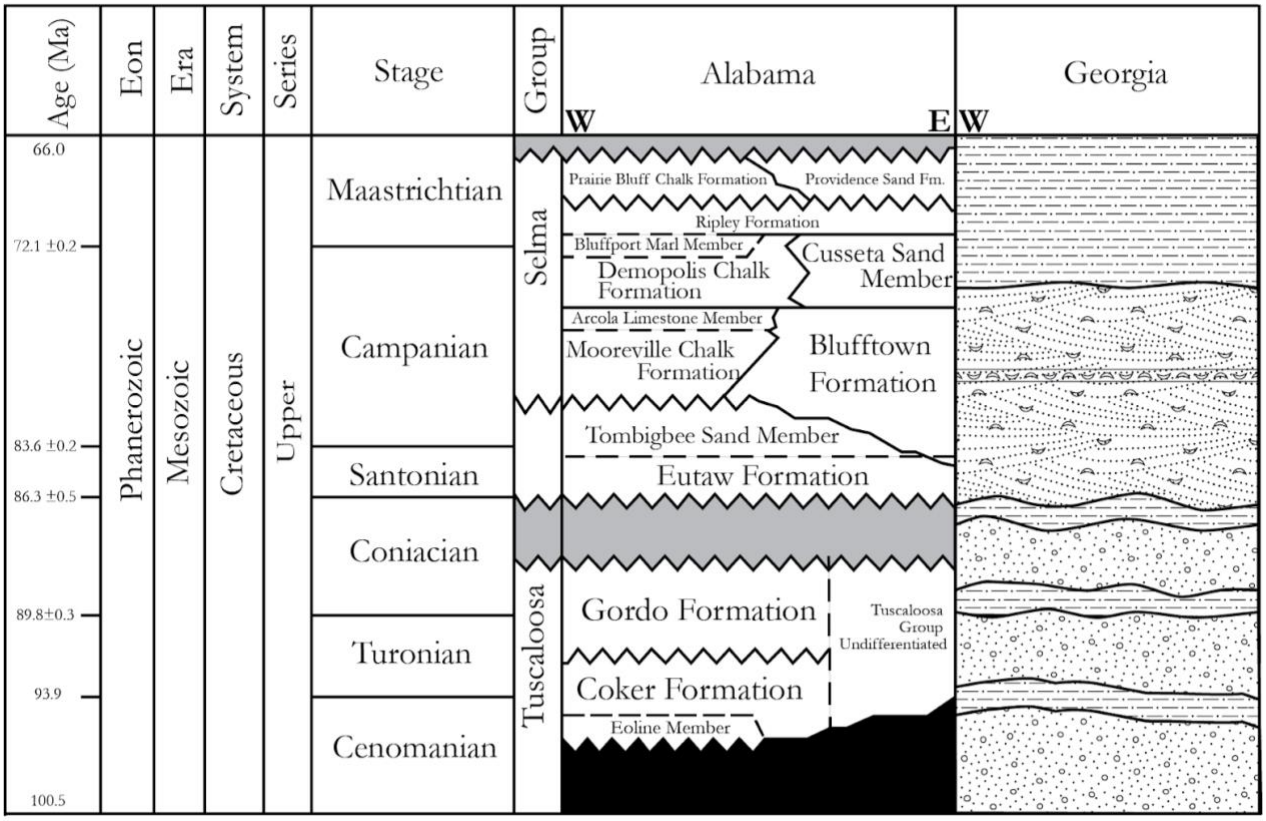

Figure 3. Upper Cretaceous stratigraphy in Alabama (adapted from Ebersole, 2013) and western Georgia (adapted from Frazier, 1982). The gray shaded areas represent missing chronostratigraphic record. The black shaded area indicates missing chronostratigraphic record at the surface.

1.2.3 Upper Cretaceous Coastal Boundary

The Eutaw Formation is not recognized in western Georgia due to paleogeographic differences. This is likely due to the formation of an estuarine area in the Chattahoochee Valley region during Late Cretaceous (Schwimmer, 2002). The fall line of the paleogeographic interpretation lies north of all samples collected in this study. Longshore drift may account for the transport of detrital zircons through the Chattahoochee valley following the southwestern paleocurrents of the Appalachian sediments. The Upper Cretaceous coastal plain boundary was connected to the western interior seaway and was likely influenced by the storm-driven, shore-parallel shelf currents found during this period (Ericksen and Slingerland, 1990). Upper Cretaceous southeasterly paleowind suggest that longshore drift may have been influenced along the Upper Cretaceous coastal plain boundary (Elder, 1988). Late Cretaceous was a time of increased storm activity due to increased temperatures and humidity levels (Hallam, 1984). There is evidence to suggest a North American monsoon during Late Cretaceous as well (Allen, 1975).

1.2.4 Eastern United States Orogenic Events

Sandstone Provenance of the Eutaw formation likely has multiple source terranes. Given the possibility of multiple sources, it is necessary to discuss every possible source available. The Eutaw Formation, being located in the eastern region of North America, was likely influenced by any or all of the known Eastern United States orogenic events which would be distinguishable in the zircon age distributions of relevant samples. There are five notable orogenic events that would be prudent to discuss, including the Grenville, Carolina, Taconic, Acadian and Alleghanian orogenic events.

The Grenville orogeny is often associated with the assembly of the supercontinent of Rodinia (Slagstad et al., 2017). Mesoproterozoic in origin, the Grenville orogenic event can be

found all over the world as a result of the breakup of Rodinia around 750 Ma (Unrug 1997). The Grenville orogenic belt can be found from Mexico to Labrador. The resulting Laurentian continent had active continental margins along its southern and eastern margins and was subducted to the northwest. This subduction which occurred from 1250 to 950 Ma likely caused enrichment of the Grenvillian lithospheric mantle (Chiarenzelli et al., 2010). The Grenville orogeny is marked by distinctive AMCG (anorthosite-mangerite-charnockite-granite) suite magmatism. Magmatic arcs formed from subduction of the active continental margins suggests a largely metamorphic source lithology commonly including amphibolite and granulite facies. Ultramafic metamorphic rocks such as Eclogite can also be seen in composition although high pressure alteration is less common (Indares and Rivers, 1995).

The Carolina terrane is a roughly 370 mile (600 km) stretch of exposed crust that runs from central Georgia to central Virginia in the United States (Secor et al., 1983). A major portion of the Carolina terrane is exposed in the eastern Piedmont Province which can be seen as far south as central Alabama (Hooper and Hatcher, 1988). The Carolina terrane is the result of subducted volcanic island arc of the Gondwanan supercontinent during the Neoproterozoic to Early Cambrian (625 to 550 Ma) (Butler and Ragland, 1969, Samson et al., 1995, Dennis and Wright, 1997). Protoliths associated with Carolina terrane included mafic, felsic, and intermediate volcanic rocks (Hibbard et al., 2002). Significant alteration of Carolina mineralogy occurred during a minimum of at least four deformational events. The Carolina terrane is the largest exotic terrane in the Appalachian region and underlies a sizeable portion of the southeastern United States (Ingle et al., 2003).

The Taconic, Acadian, and Alleghanian orogenic events are often referred to as Appalachian orogeny as all three orogenic events influenced the Appalachian mountains in

various chronological stages. The first of the three orogenic events, the Taconic orogeny formed much of modern day New England. After the Iapetus Ocean closed roughly 550 Ma, accumulated sediment weight working in parallel compressional crustal forces, depressed the eastern edge of the North American continent into a downward fold. Shallow water carbonate deposition was replaced with fine-grained clastic deposition along this continental shelf margin, eventually increasing sediment deposition depth. A small volcanic island chain developed along the eastern edge of a convergent plate boundary which was then subducted (www.usgs.gov). The subduction continued in an eastern direction eventually dewatering the subducted plate which lowered the melting point of peridotites in the overlying mantle wedge. These partially melted peridotites returned to the surface in the form of the Taconic island arc (www.usgs.gov). The Taconic island arc collided with the North American continent at some point in the Late Ordovician causing intense folding and faulting along with periods of extreme metamorphism.

The second of three mountain-building events forming the Appalachian Mountains in eastern North America, the Acadian orogenic event is believed to have occurred roughly 375 to 325 Ma (Ryder et al. 2008). The Acadian orogenic belt extended from Newfoundland in a southwesterly direction toward Alabama (Ettensohn, 1987). What began as a depositional fore-arc basin, the Acadian orogeny folded the basin as a mountain chain gradually compressing crustal material in a westward direction throughout the Devonian eventually influencing the western margins of the Late Devonian Appalachian geosyncline. The Acadian orogeny is believed to have been caused by the collision of Avalonian continental fragments with the Laurasian continent producing an eastward subduction of the proto-Atlantic. The Acadian orogeny was responsible for a large amount of angular unconformities and igneous intrusions. Among these included regional

metamorphism and deformation of Devonian rocks. Source rock lithology of the Acadian orogenic event can be seen through this regional metamorphism.

The final of three mountain-building events forming the Appalachian Mountains in eastern North America, the Alleghanian orogenic event is believed to have occurred roughly 325 to 260 Ma (Ryder et al. 2008). The Late Paleozoic collision of North Africa and the southern and central Appalachian continental margin of North America caused the Alleghanian orogenic event. Evidence of the Alleghanian orogeny is best exhibited in the southern and central Appalachians where the westward thrusting of the Blue Ridge mountains and compressional folding and faulting of the Ridge and Valley Province can be seen. Igneous intrusions and metamorphism are common in the Piedmont province as well. Source rock lithology for the Alleghanian orogeny is largely crystalline featuring igneous and metamorphic rocks. This is especially true for the Piedmont, Blue Ridge, Adirondack, and New England Provinces who are commonly referred to as the Crystalline Appalachians (Wenner, 1981).

1.2.5 Concerning Zircons

Zircon ($ZrSiO_4$) is a prominent refractory mineral belonging to the nesosilicates group. It is a rather tough mineral able to withstand temperature up to 1690º C and pressures up to 4.8 GPa without physical or chemical alteration (Finch and Hanchar, 2018). Due to their robust nature zircon minerals often survive partial melting of their host rocks and retain their original composition and are useful for provenance studies (Gehrels, 2014; Zhang et al., 2016; King et al., 2019). Being a common accessory mineral, zircon can be found in igneous, metamorphic, and sedimentary rocks. Zircon is best known for its significance in the field of geochronology. This largely due to the fact that zircon incorporates radioactive uranium (U) during crystallization but

minimal lead (Pb). The uranium steadily decays over geologic time into radiogenic lead, which provides a means for isotopic age dating (Scherer et al., 2007).

As the need for accurate age dating has increased in recent history, zircon has become a prominent mineral for geochronological dating. Zircon has even played a key role in isotopically dating the age of the Earth (Dalrymple, 1994). This study will focus on the occurrence of detrital zircon found within the Upper Cretaceous Eutaw Formation and will utilize zircon in an effort to investigate the sandstone provenance of the formation as it relates to the surrounding regional stratigraphy.

Detrital zircon geochronology focuses on instances where the accessory mineral has been worn out of pre-existing source rocks through processes of weathering and/or erosion. Zircon included within sandstone such as the Eutaw Formation is often detrital in nature as any accessory minerals will have been included during the formation of the sedimentary host rock. If these detrital zircons can be accurately age dated implications can be made as to what pre-existing source rocks detrital zircons were transported from originally.

1.2.6 U-Pb Zircon Geochronology

The importance of radiometric dating cannot be overstated in pursuing geochemical insights within the Upper Cretaceous coastal plain boundary. Through the use of zircon, the decay rates of radioactive isotopes associated with the formation of the mineral allow for an accurate age determination. It is understood that radioactive parent isotopes decay at constant rates through time into daughter isotopes. These constant rates of decay are referred to as half-lives, which refers to the time necessary for half of the parent isotope to decay into a daughter isotope. The probability of decay per unit time is known as the decay constant or rate of decay (Zou, 2007). Because the decay constant is isotope specific and not influenced by external conditions such as

pressure or temperature, geologists are able to create a fairly accurate natural clock for determining the quantitative age of a rock. This natural clock is the foundation of radiometric dating. Unfortunately, in some cases, daughter isotopes may be incorporated into the initial composition of the mineral which requires a correction where the initial daughter isotopes are removed from the age calculation. Because Zircon has minimal to no Pb during the initial formation, the mineral provides a means of accurate and precise isotopic age determination (Scherer et al., 2007).

Although there are isotopic series better suited to other tasks, U-Pb Decay is a very common isotopic series found in radiometric dating. This is largely due to the extended time range afforded by the series. The U-Pb Decay isotopic series has several intermediate isotopes before reaching stability finally at ^{206}Pb (Figure 4). As an example of the extended range, U-Th isotopic series (^{238}U-^{230}Th) has a half-life of 75,960 years, while the U-Pb isotopic series (^{238}U-^{206}Pb) has a half-life of 4.5 Ga (Tucker, 2011). The short-lived ^{238}U-^{230}Th disequilibrium has been used to date young (<0.375 Ma) zircons (e.g., Zou et al., 2014, 2020). The long-lived U-Pb isotopic series (^{238}U-^{206}Pb) has been used extensively to date zircons older than 0.375 Ma. Because detrital zircons in this study are old, we employ ^{238}U-^{206}Pb for zircon dating.

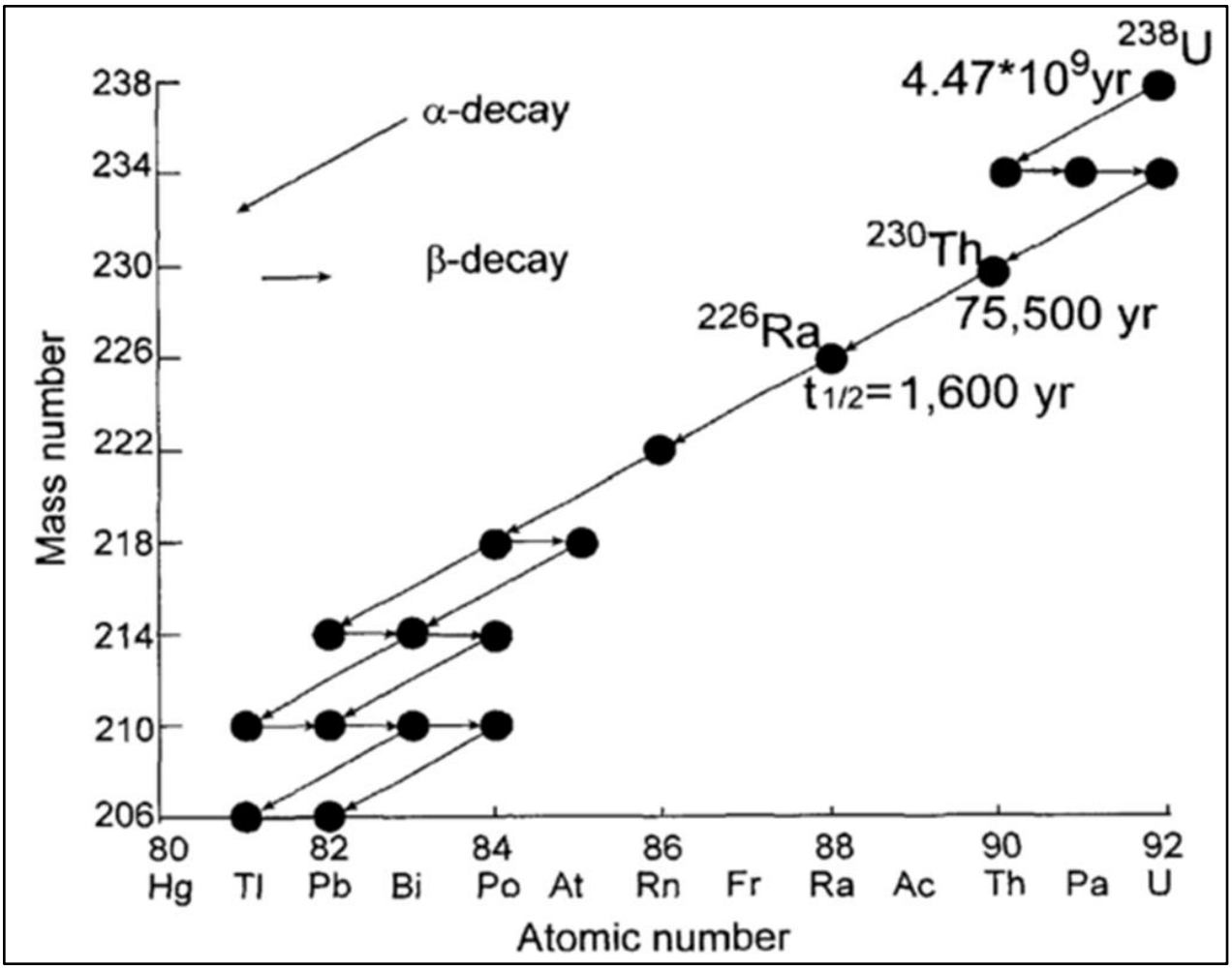

Figure 4. Decay series of ^{238}U to the final stable ^{206}Pb showing intermediate isotopes ^{230}Th and ^{226}Ra, $t_{1/2}$ denotes half-life (Zou et al., 2007).

1.2.7 Secondary Ion Mass Spectrometry (SIMS)

Secondary ion mass spectrometry (SIMS) is a commonly utilized radiometric technique that analyzes the composition of solid surfaces. Since its discovery in 1910 by J.J. Thompson, SIMS has really become an accurate and often cited radiometric dating technique. This technique is often accomplished using an ion microprobe by sputtering the surface of the sample with a primary ion beam generated in a duoplasmatron (Ireland and Williams et al., 2003). The ejected

secondary ions reflected off the surface of the sample are collected and analyzed as a function of their mass-to-charge ratio (Schwarz, 2001). The increased depth resolution associated with sputter depth profiling and the high sensitivity achievable by individual ion detection makes SIMS analysis a commonly used radiometric dating technique.

This research employs SIMS by sputtering samples with a primary ion beam of $^{16}O^-$ ions at sputter rates of ~0.05 µm/nA/sec (Zou et al., 2010; Tucker et al., 2013). After sputtering a sample with $^{16}O^-$ ions, the small percentage of secondary atoms ionized in the process are then accelerated in a mass spectrometer where tabulation of the data occurs (Figure 5). When combined with surface imaging techniques (e.g. backscattered electron and cathodoluminescence), SIMS is able to focus on particular areas of interest on the exposed crystal surface (Figure 6). These surface imaging techniques allow for isotopic analysis of the sample.

SIMS dating is highly sensitive to most elements in the periodic table, occasionally in the parts-per-billion range (Schwarz, 2001). Therefore, in order to ensure SIMS does not record data erroneously, certain precautions must be taken. This is to mitigate a variety of complications that range from errors in sample preparation to instrumental errors. To minimize the risk of error, unknown zircon samples are mounted with known zircon standards. Using the known zircon ages of these mounted standards, errors with the ion microprobe can be identified and corrected if necessary before proceeding with the prepared samples. Although zircon has minimal to no Pb during the initial formation, common Pb concentrations must be tested and corrected for in order to achieve an accurate age (Scherer et al., 2007). The presence of Pb in zircon can be acquired from a variety of sources including laboratory Pb from polishing compounds, laboratory Pb from coating materials, microscopic mineral inclusions, and Pb added to the zircon during or after the alteration occurs. This contamination can adversely affect the accuracy of age data if not properly

corrected for. In order to combat potential contamination sources. Equation 1 and Equation 2 can be used to estimate common Pb content (Zou, 2007).

Eq. 1

$$f = {}^{206}Pb_{initial}/{}^{206}Pb_{total}$$

Next *f* can then be calculated as,

Eq. 2

$$f = \frac{\left({}^{204}Pb/{}^{206}Pb\right)_{total}}{\left({}^{204}Pb/{}^{206}Pb\right)_{initial}}$$

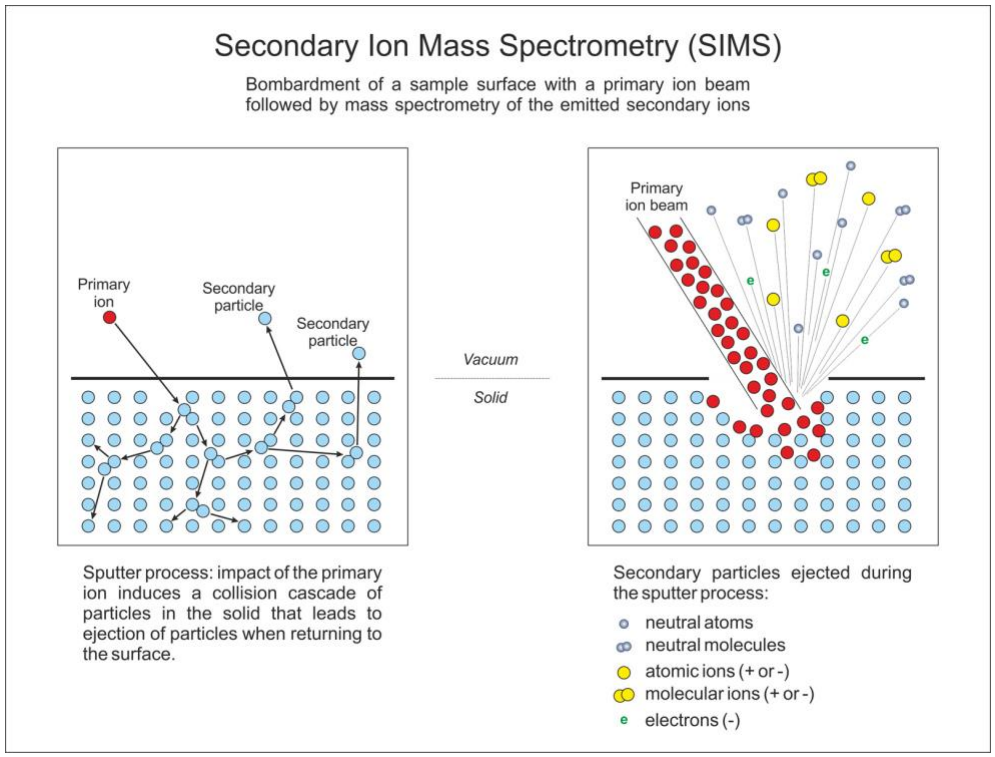

Figure 5. Diagram depicting a sample being sputtered by a beam of primary ions, resulting in the backscatter of secondary atoms, molecules, and ions (Heidelberg University 2017)

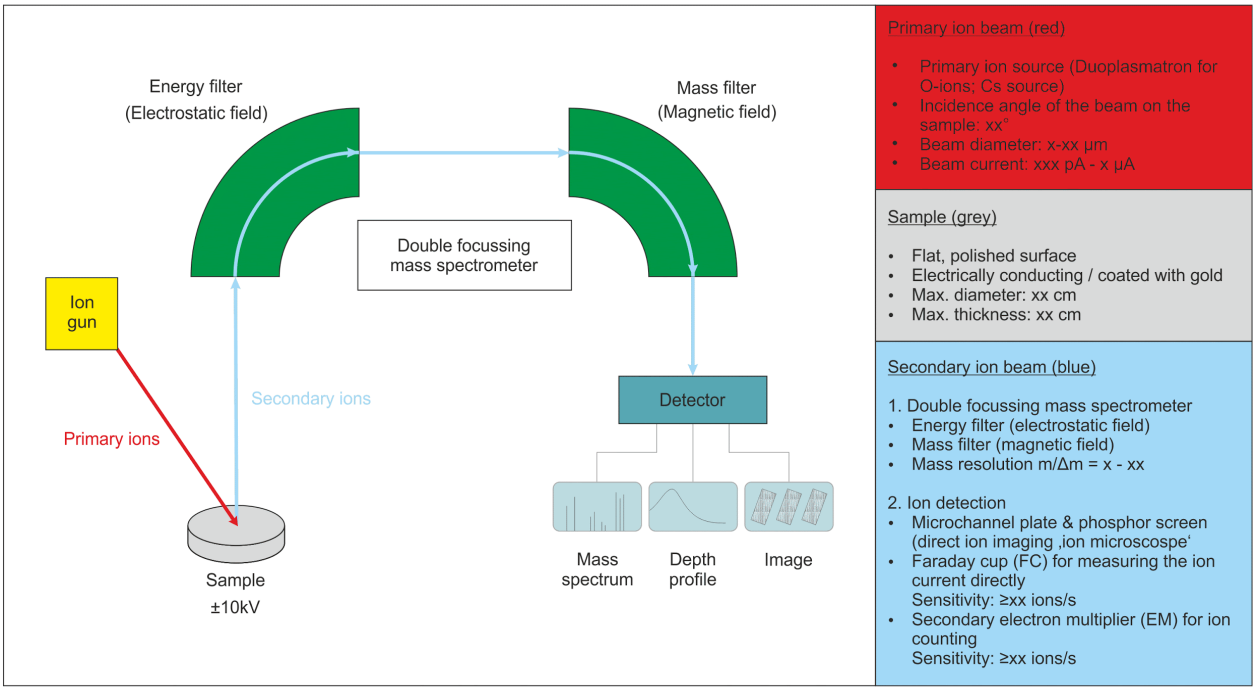

Figure 6. Simplified schematic diagram of SIMS and three different modes of localized analysis (Heidelberg University 2017)

When compared to other radiometric techniques, SIMS analysis has some very distinct benefits. SIMS analysis is often regarded as the least destructive dating technique available. This is an especially accurate statement when compared to Thermal Ionization Mass Spectrometry (TIMS) and Laser Ablation Inductively Coupled Plasma Mass Spectrometry (LA-ICP MS) (Figure 7). TIMS analysis, in particular, entirely consumes the sample (Košler and Sylvester, 2003). The total sampling depth associated with SIMS analysis is less than 5 µm on average with a target area ranging from 10 to 50 µm in diameter (Ireland and Williams, 2003). Another benefit of SIMS analysis is the minimal heating and vaporization associated with the technique as a much lower amount of energy is absorbed by the target sample (Stern, 2009).

If mounted properly, the Pb/U age of zircon can be accurately measured down to a few hundred thousand years by measuring radiogenic Pb concentrations down to a few parts-per-billion. Accuracy of samples can be further improved by utilizing longer counting times and ensuring that Uranium rich zones are targeted during analysis. While TIMS analysis may allow for more precise results when not sampling such a small volume of material, SIMS analysis is particularly useful in U-Pb dating with unrivaled accuracy and precision at an intra-crystalline scale (Ireland and Williams, 2003).

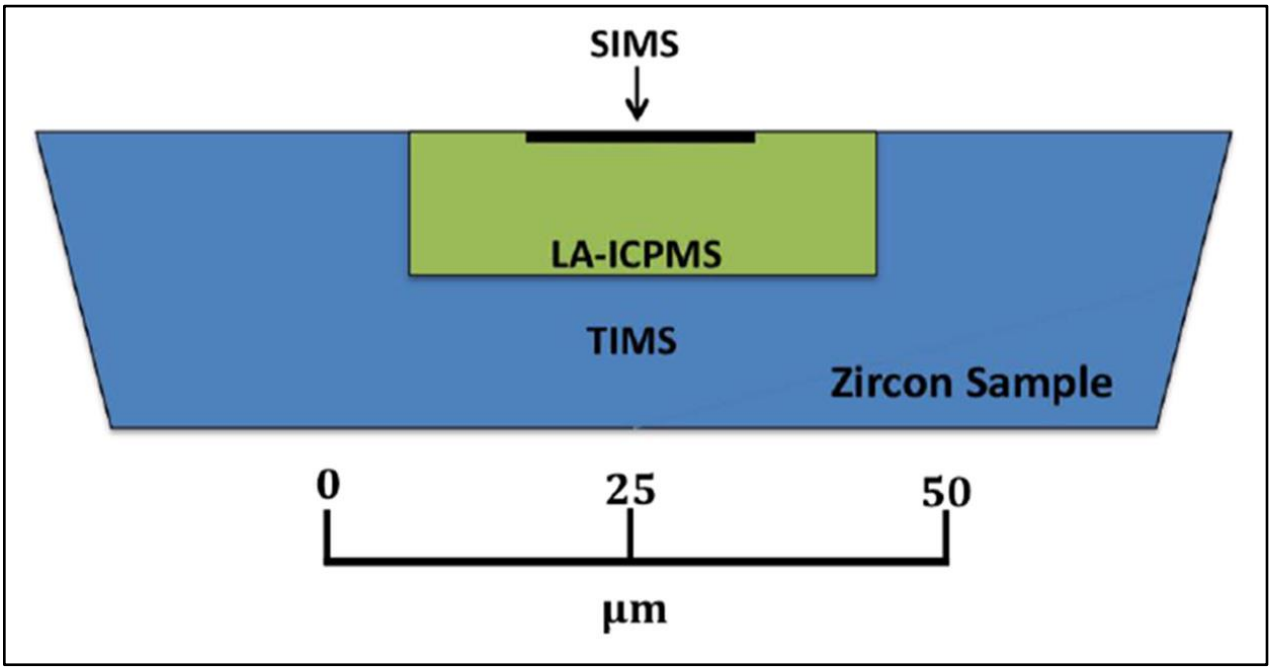

Figure 7. Schematic diagram comparing average zircon sample destruction area of SIMS, LA-ICP MS, and TIMS in cross-section view. Note that SIMS spot size is ~10-20 μm and <2 μm depth. LA-ICPMS spot size is ~30-60 μm and 10-20 μm depth (Košler and Sylvester, 2003).

1.3 Previous Studies

1.3.1 Late Cretaceous Paleoclimate

Paleogeographic characteristics of the Alabama/Georgia state border contributed to sedimentation of the Eutaw Formation by enabling longshore drift along the coastal plain boundary during Late Cretaceous (Schwimmer 2002). Reconstructed paleoenvironment data of the coastal plain boundary (middle-Campanian) confirms the possibility for longshore drift (Figure 8). There is data to suggest the possibility of a long-lived (~10 to 28 m.y.) drainage system in the vicinity of the modern lower Chattahoochee River valley area (Black et al., 2015) which may confirm possible longshore drift of detrital zircon. Evidence of the accessory mineral, zircon, was confirmed in a mineralogical study conducted by Osborne (2013). Detrital zircon samples were collected from sample locations chosen on the advice of C. Savrda (personal communication, 2019) and the cartographic work of Szabo et al. (1988).

The Upper Cretaceous (upper Santonian-Maastrichtian) saw increased temperatures and humidity globally (Hallam,1984). Upper Cretaceous temperatures likely increased storm surges globally including monsoonal winds (Allen, 1975). There is also evidence to suggest that sea-level changes may have disturbed sediment deposition of the Eutaw Formation during the Upper Cretaceous (King, 1990). There is a possibility that longshore drift of detrital zircons may have been disturbed due to the climatic conditions during Late Cretaceous (late Santonian-Maastrichtian).

Davis (1988) correlates the Eutaw Formation to surrounding strata with a broad overview of the stratigraphic and hydrogeological framework of the Alabama coastal plain. The Tombigbee Sand Member unconformably contacts the Mooreville chalk, which is highlighted by a bed of

glauconitic, chalky sand (Stephenson and Monroe, 1938). This data helps define a well-rounded picture of the topic area sandstones that will be subjected to radiometric dating techniques.

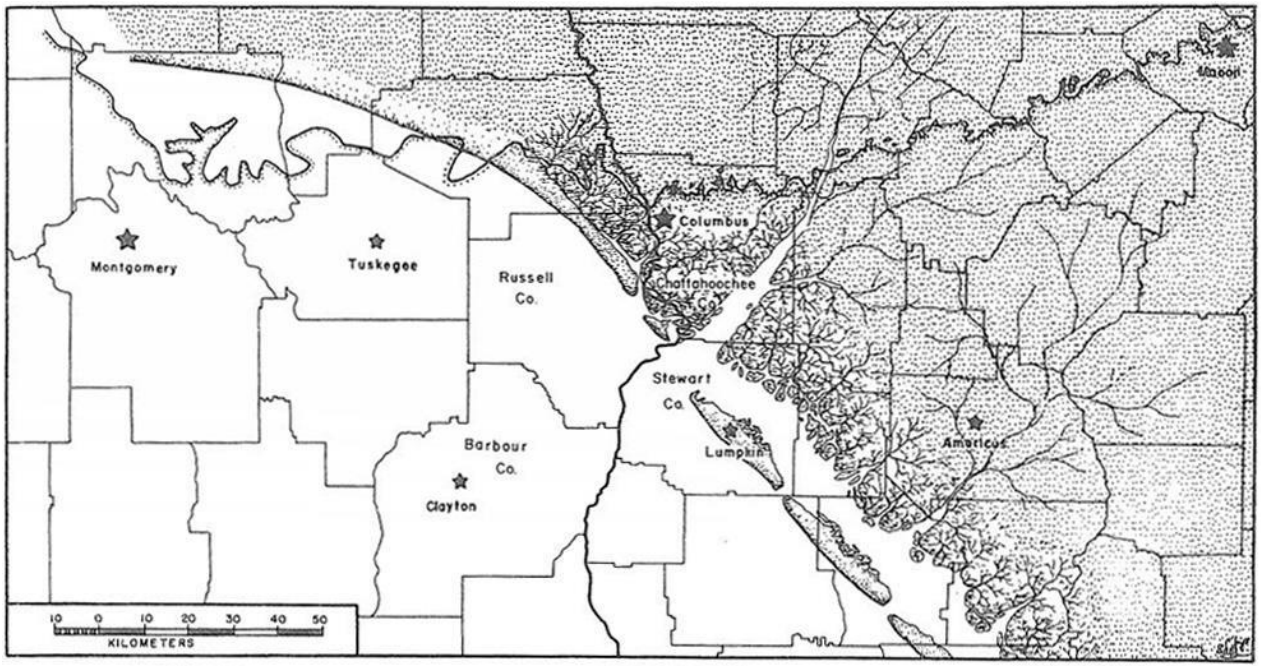

Figure 8. Reconstruction of the paleoenvironment of the southern coast of western Georgia and eastern Alabama, during the middle Campanian (Schwimmer, 2002).

RESEARCH

2.1 Sampling

Four exposures were sampled in order to analyze the Tombigbee Sand Member and its place within the Eutaw Formation. Samples were collected from both central and eastern Alabama in Montgomery, Muscogee, and Russell counties respectively. The nomenclature of samples is defined as the year of collection, the closest regional airport code, and the order in which samples were collected in the focus area.

2.1.1 19MGM-1

This sample was originally collected from the “Sand Hill" locality found slightly off Hayneville Road in northwest Montgomery County, Alabama (Figure 9). Although it no longer exists, this inner Coastal Plain outcrop was located on the margins of a cap-rock protected knoll (King, 2003). Sand Hill served as a foundation for understanding the facies history of the Tombigbee Sand Member of the Eutaw Formation and was known for its vertebrate fauna with excellent physical and ichnologic sedimentary structures. Sand Hill is located just east of Catoma Creek, a well-known source of vertebrate fossils such as the Coelacanth fish (Figure 10) (Scwhimmer, 1994). Beginning, just north of the Montgomery Regional Airport, Catoma Creek is roughly 41 miles in length encompassing a total drainage area of nearly 360 square miles (Alabama Department of Environmental Management, 2005). Sample 19MGM-1 was analyzed by XRD for bulk mineralogy. The ICP-AES and ICP-MS were utilized for major and trace elemental composition analysis. Sample 19MGM-1 was analyzed for use in SIMS analysis as well.

Figure 9. Sand Hill Locality, sample site of 19MGM-1. Photo from King (2003).

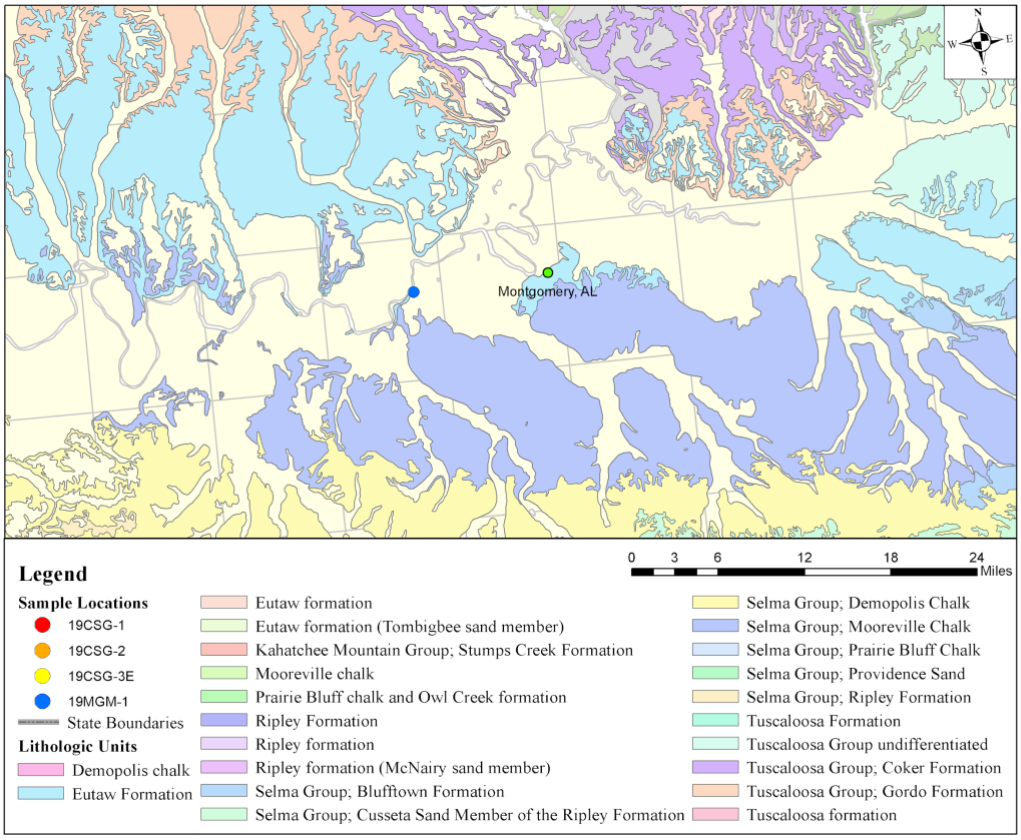

Figure 10: Geologic map with a focus of Catoma creek

2.1.2 19CSG-1, 19CSG-2, 19CSG-3E

Three samples were collected from focus unit exposures in the Phenix City, AL, and Columbus, GA region (Figure 11). Samples within Muscogee County and Russell County were collected approximately 100 miles from the Catoma Creek sample site. Collected sample sites for 19CSG-1 and 19CSG-2 are exhibited in Figures (12, 13) respectively. Sample 19CSG-2 was collected behind the Commando Military Supply along Victory Drive in Columbus, Georgia. All samples were analyzed via XRD bulk mineralogy. ICP-AES and ICP-MS were utilized for major and trace elemental composition analysis. All samples were analyzed for use in SIMS analysis as well.

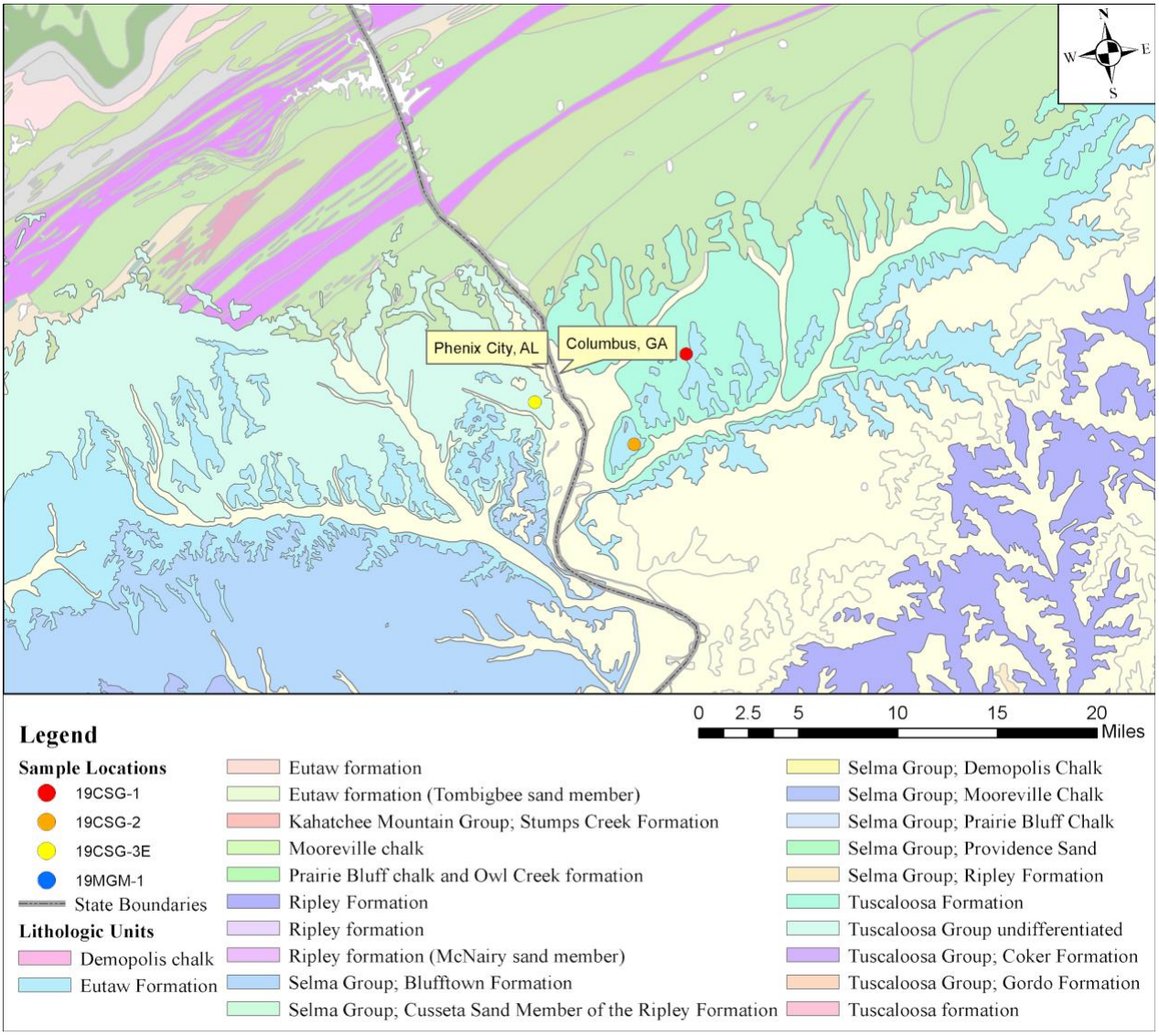

Figure 11. Geologic map with sample collection sites along the Alabama-Georgia border.

Figure 12. Sample collection site of 19CSG-1 in Columbus, GA

Figure 13. Sample collection site of 19CSG-2 in Phenix City, AL

2.2 Methods

2.2.1 Grain Size Analysis

Four representative samples of the Eutaw Formation were analyzed for their grain-size parameters and statistical relationships. Each sample featured grain sizes ranging from very coarse sand to silt with varying degrees of sorting. 300 mL of each sample was measured and used during grain-sieve analysis. Grain-size classes were determined using the Udden-Wentworth grade scale (Table 1). The dimension of grain-sizes (millimeters) was converted to a phi scale which is a logarithmic scale to base 2.

Eq. 3 $$\emptyset = -\log_2 D$$

where ∅ is the phi size and D is the grain diameter in millimeters.

The results of the grain-size analysis were graphically represented in the form of volume percentage curves (Figure 19). Statistical analysis of grain-size data referencing the cumulative curves was used to describe the grain-size distribution mathematically (Figure 20).

Table 1. Udden-Wentworth Scale

Grain Size (mm)	Phi Standard Deviation (∅)	Grain Size
2	-1	Very Coarse Sand
1	0	Coarse Sand
0.5	1	Medium Sand
0.25	2	Fine Sand
0.125	3	Very Fine Sand
0.0625	4	Coarse Silt

2.2.2 X-ray Diffraction Geochemical Analysis (XRD)

All samples collected were analyzed using x-ray diffraction (XRD) in order to determine bulk mineralogy. Samples were ground for a duration of roughly 10 minutes using a Torrey Hills Planetary Ball Mill with steel grinding containers until fully powdered. Powdered samples were pressed into sample casings and analyzed using the Bruker D2 Phaser at the Auburn University XRD Lab (Figure 14). Samples underwent X-ray diffraction at 2θ angles between a range of 5° and 75°. The step time for each sample was ~51 seconds, for a total sample analysis time of approximately 60 minutes per sample. Concentrated x-ray beams were sputtered through a 20 mm brass slot and reflected onto an LYNXEYE XE-T detector™. Peaks were identified using the COD (Crystallography Open Database) reference library as part of the DIFFRAC.SUITE EVA Xrd Software Program. Mineral percentages were then determined using reference intensity ratios (RIR). The Reference Intensity Ratio (RIR) is a method used for Quantitative Analysis by Powder Diffraction, where analysis is based on scaling all diffraction data to the diffraction of standard reference. In the case of detrital samples, quartz is often referenced as the diffraction standard due to the mineral's increased durability. Interpretation of RIR helps identify observed mineral suites, mineral exclusions, and the relevant abundances of different mineral phases. Uncertainty of relative abundances varies relative to the chosen reference standard.

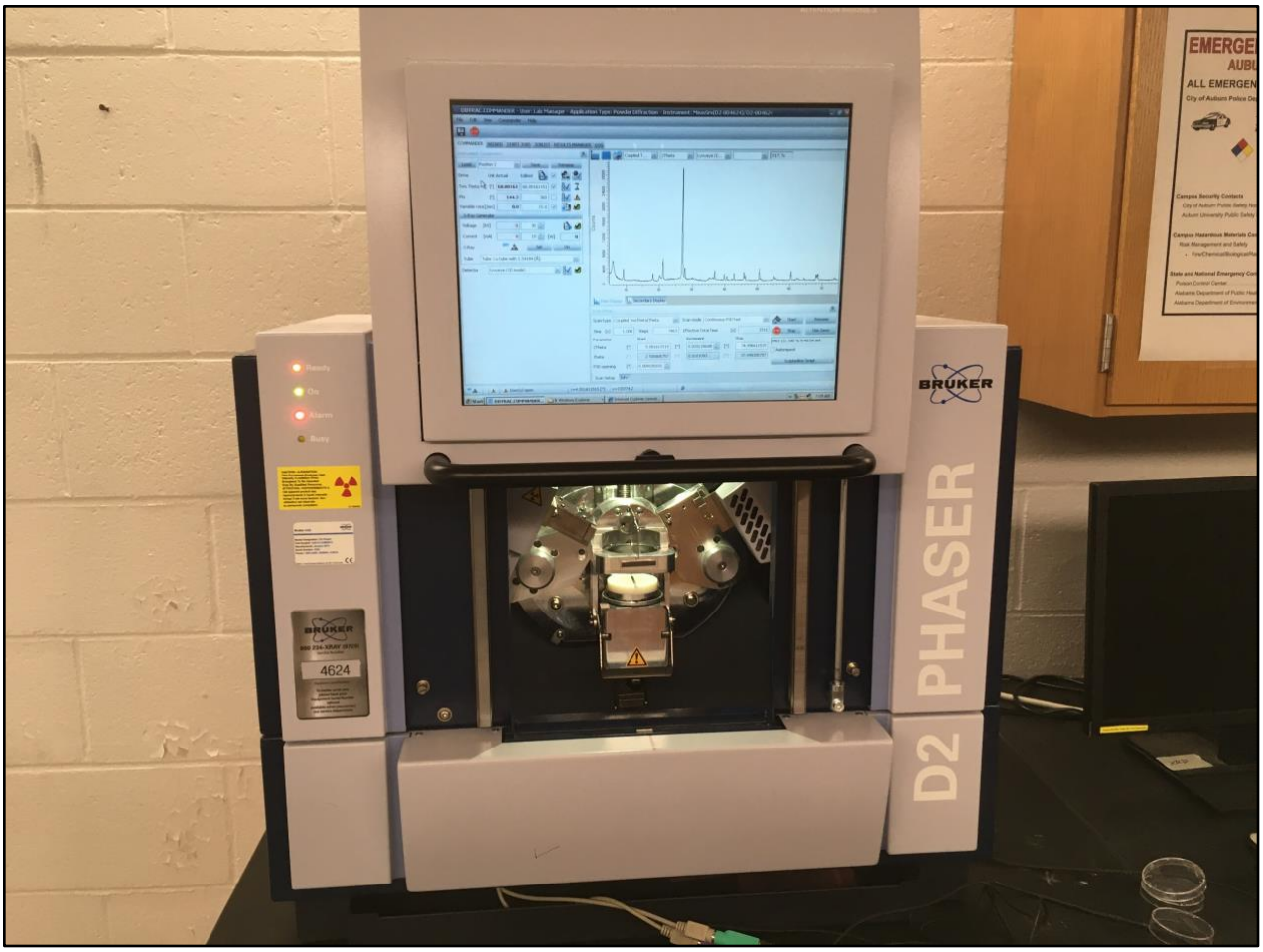

Figure 14. Bruker D2 Phaser at the Auburn University XRD Lab

2.2.3 ICP-AES (Inductively Coupled Plasma Atomic Emission Spectrometry)

Whole rock analysis was implemented using ICP-AES (ICP Atomic Emission Spectrometry). ICP-AES is a spectral method used to determine very precisely the elemental composition of samples; it can also be used to quantify the elemental concentration with the sample (www.libretexts.org, 2020). ICP-AES utilizes the energized plasma from an inert gas such as argon to rapidly burn analytes. Emitted analyte colors are indicative of present elements, and the concentration of present elements are represented by the color intensity.

Utilization of high-energy plasma to emit photons from excited analytes enables ICP-AES whole rock analysis. An inert gas, such as argon, passes through an alternating electric field induced by an inductively coupled coil creating high energy plasma (Figure 15). The excited analyte dissipates the induced energy by moving electrons to a lower energy state, which emits excess energy in the form of light. The wavelength emitted represents the energy gap between the excited energy level and the ground state. These energy gaps are elementally specific based on electron orbital configuration and the number of electrons in an element. Therefore, by utilizing the wavelength of light, the present elemental composition can be determined. The energy gap between the excited state to the ground state can be represented in Equation 4 where ΔE dictates the color of the light or wavelength of the light, h is Planck's constant (6.626×10^{-34} m^2kg/s), and ν is the frequency of the emitted light.

Eq. 4 $$\Delta E = h\nu$$

Through wavelength detection, ICP-AES can detect present elemental composition. Beyond wavelength detection, the intensity of emitted light is indicative of elemental concentrations as well. Intensity is correlated to elemental concentration.

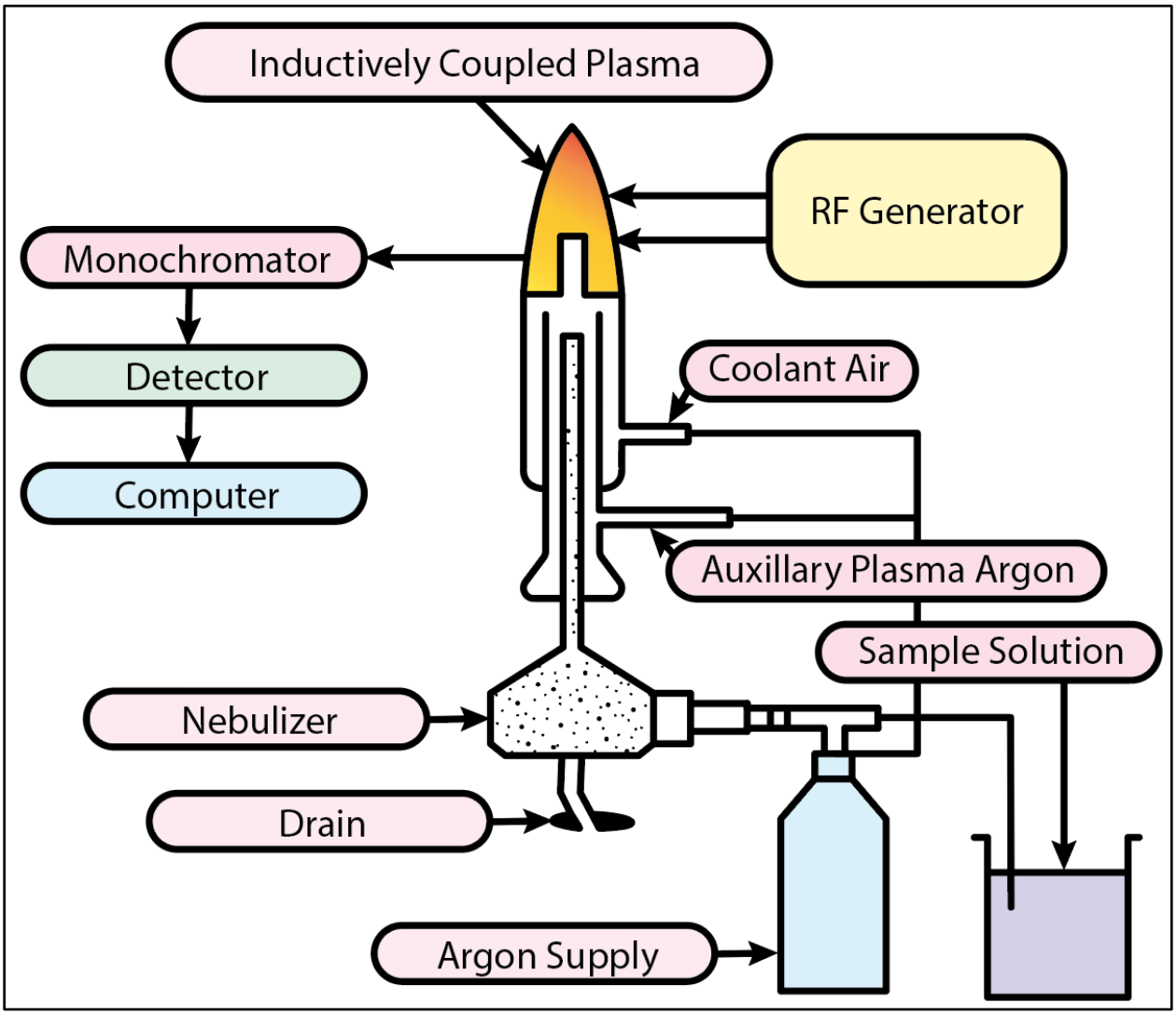

Figure 15. Schematic of an ICP-AES (ICP Atomic Emission Spectrometry)

2.2.4 ICP-MS (Inductively Coupled Plasma Mass Spectrometry)

Trace element analysis was implemented using ICP-MS (Inductively Coupled Plasma Mass Spectrometry). ICP-MS is an analytical technique for determining trace multi-elemental and isotopic concentrations in liquid, solid, or gaseous samples (www.libretexts.org, 2020). ICP-MS combines the sensitive detection limit of mass spectrometry detection with an ion-generating argon plasma source. Lithium borate fusion was followed by ICP-MS analysis to generate trace element suites.

Although ICP-MS is often compared to ICP-AES, there are significant differences between techniques. The primary difference between ICP-MS and ICP-AES is how ions are generated and detected. Unlike ICP-AES, which excites ions with vertical plasma into emitting photons separated by wavelength emissions, ICP-MS excites ion with horizontal plasma based on their mass-to-charge ratios (m/z) (Figure 16). The differences in detection methods and ion formation impacts the sensitivities of both methods. ICP-MS has a detection limit of a few ppt to a few hundred ppm, compared to the ppb-ppm range (~1 ppb - 100 ppm) of ICP-AES (www.libtexts.org, 2020). Both methods utilize very fast, high throughput multi-elemental analysis (~10 - 40 elements per minute per sample). Additionally, ICP-MS is a more precise method utilizing a detection level of eight orders of magnitude over ICP-AES' six. ICP-MS alone is enabled to differentiate between elemental isotopes due to its ability to segregate ions based on mass.

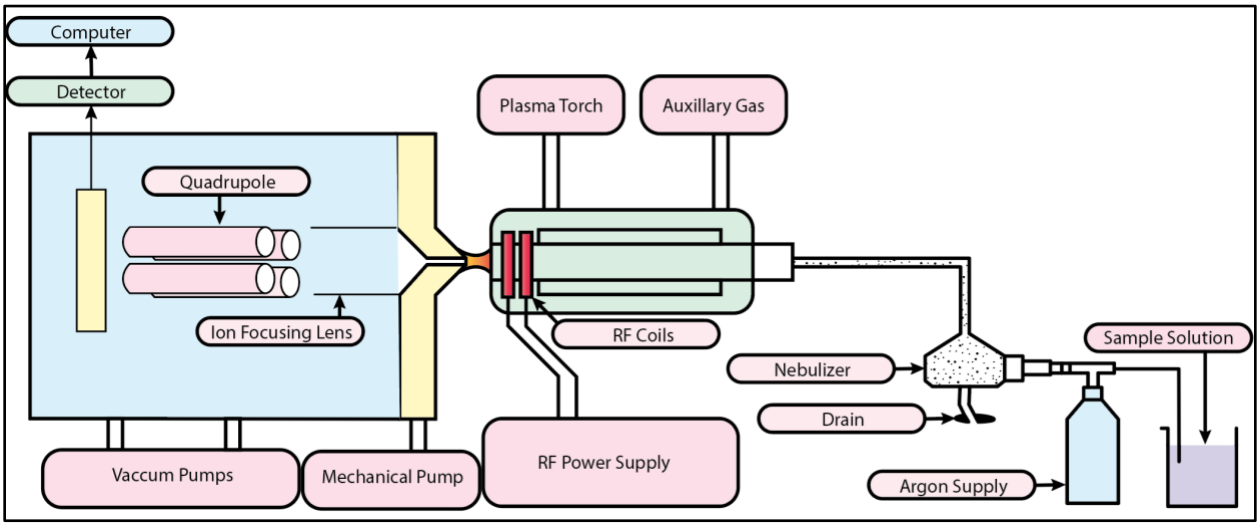

Figure 16. Schematic of an ICP-MS (Inductively Coupled Plasma Mass Spectrometry)

2.2.5 Uranium-Lead (U-Pb) Isotopic Analysis

SIMS dating is highly sensitive to most elements in the periodic table, occasionally in the parts-per-billion range (Schwarz, 2001). Therefore, in order to ensure SIMS does not record data erroneously, certain precautions must be taken. A majority of mitigation requires meticulous sample preparation. Care was taken to faithfully minimize potential uncertainty during the preparation process at the NSF National Ion Microprobe Facility hosted at UCLA. The goal of sample preparation in SIMS is to create sample mounts that can be utilized in the Cameca IMS-1290 Microprobe. Secondary ion yields are sensitive to local topographic and electrostatic features of the sample mount further emphasizing the necessity of proper preparation methods (Stern, 2009).

After zircon extraction, a fine-point needle is used to select and place zircon grains onto a piece of double-sided tape. Depending on the necessary requirements of the experiment, a variable amount of zircon grains may be required for analysis. Any zircon grains meant to undergo SIMS dating will be placed in rows upon the tape. A Teflon® mold is then placed around the zircon grains so that an epoxy mixture can be poured into the mold itself. The epoxy mixture takes approximately 24 hours to dry. Once the epoxy mixture is considered dry, the double-sided tape and the mold are removed from the sample. Dry epoxy must be shaved down to an appropriate thickness for analysis. To minimize error, the shaved epoxy sample will be polished to ensure a smooth, flat, and exposed zircon grain surface. This method is a synthesis of the techniques noted by Ireland and Williams (2003), Grove et al. (2008), and Cooper (2016).

Once mount preparations are complete, the last step is to wash the epoxy with dilute HCl at 5%, methanol, and soapy water, and then dry it in an oven. Once dry and clean, the epoxy mount is gold-plated to generate a conducting surface (Figure 17). Ion probes are kept under

ultra-high vacuum (UHV), requiring the mount must be placed into a sample holder through an airlock system. In order to generate U-Pb ages from each zircon, each sample must be sputtered with a beam of ($^{16}O^-$) primary ions. The machine that will be utilized in this study is the IMS-1290 (Figure 18) at the UCLA NSF Facility. When SIMS analysis is complete, the epoxy mount containing all preparatory work may be kept for future analysis.

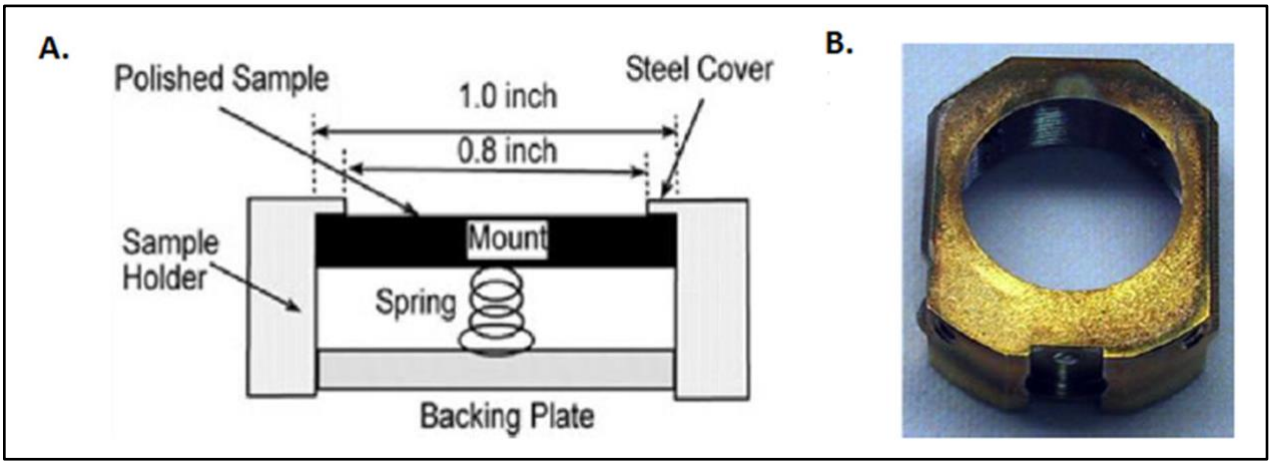

Figure 17. (A.) Schematic diagram of a sample holder showing the backing plate and spring. Note that the amount of mount surface area available for analysis is decreased by 0.2 inches after insertion into the sample holder (UCLA, 2020). (B.) Photograph of a standard sample holder (Cooper, 2016)

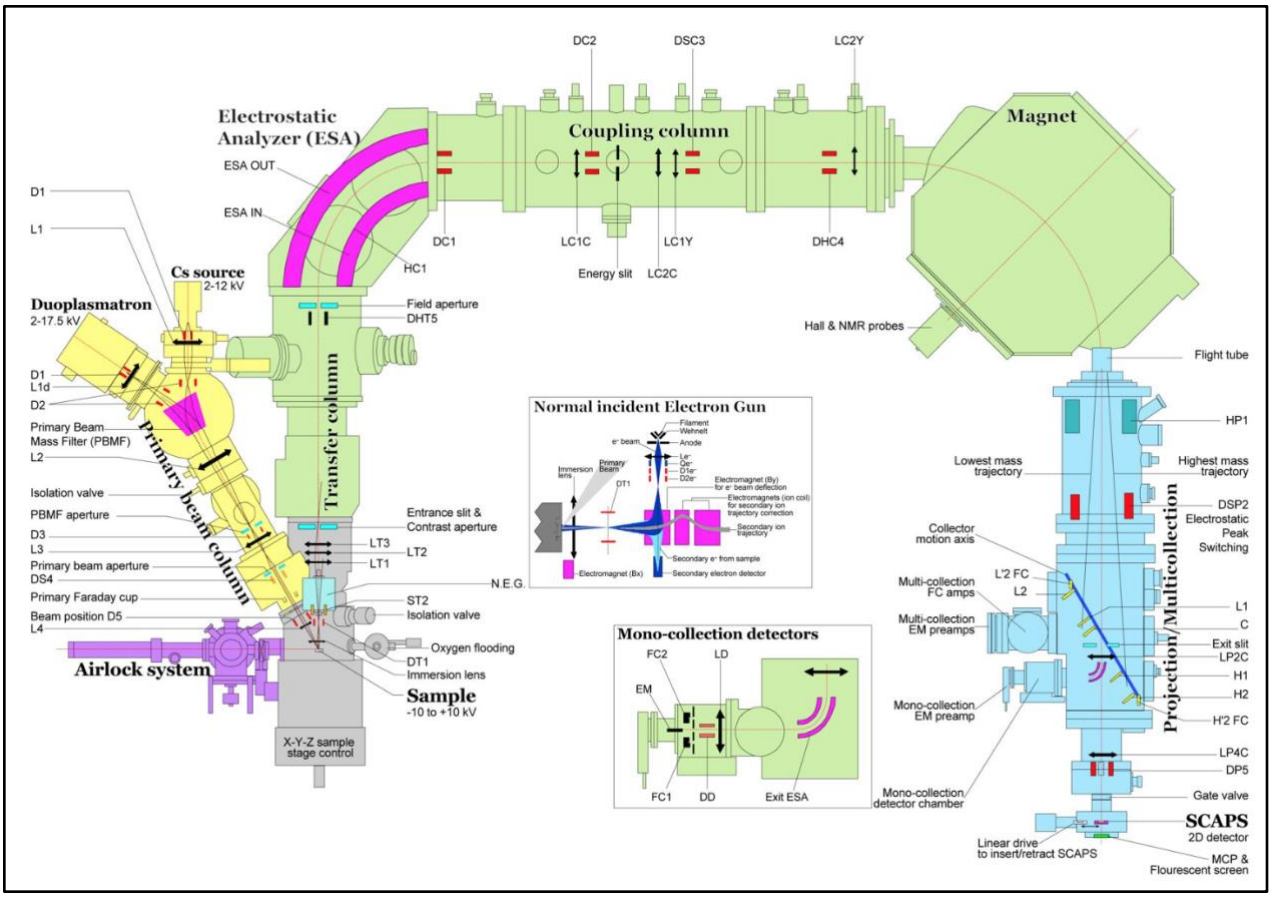

Figure 18. Schematic overview of the CAMECA IMS-1290 (UCLA, 2020).

RESULTS

3.1 Grain Size Analysis Results

The peak Phi values are 2 for 19MGM-1 and 19CSG-1, 4 for 19CSG-2, and 3 for 19CSG-3E. Samples 19MGM-1 and 19CSG-1 have the largest grain size and are selected for zircon separation. Sample 19CSG-2 has the smallest grain size.

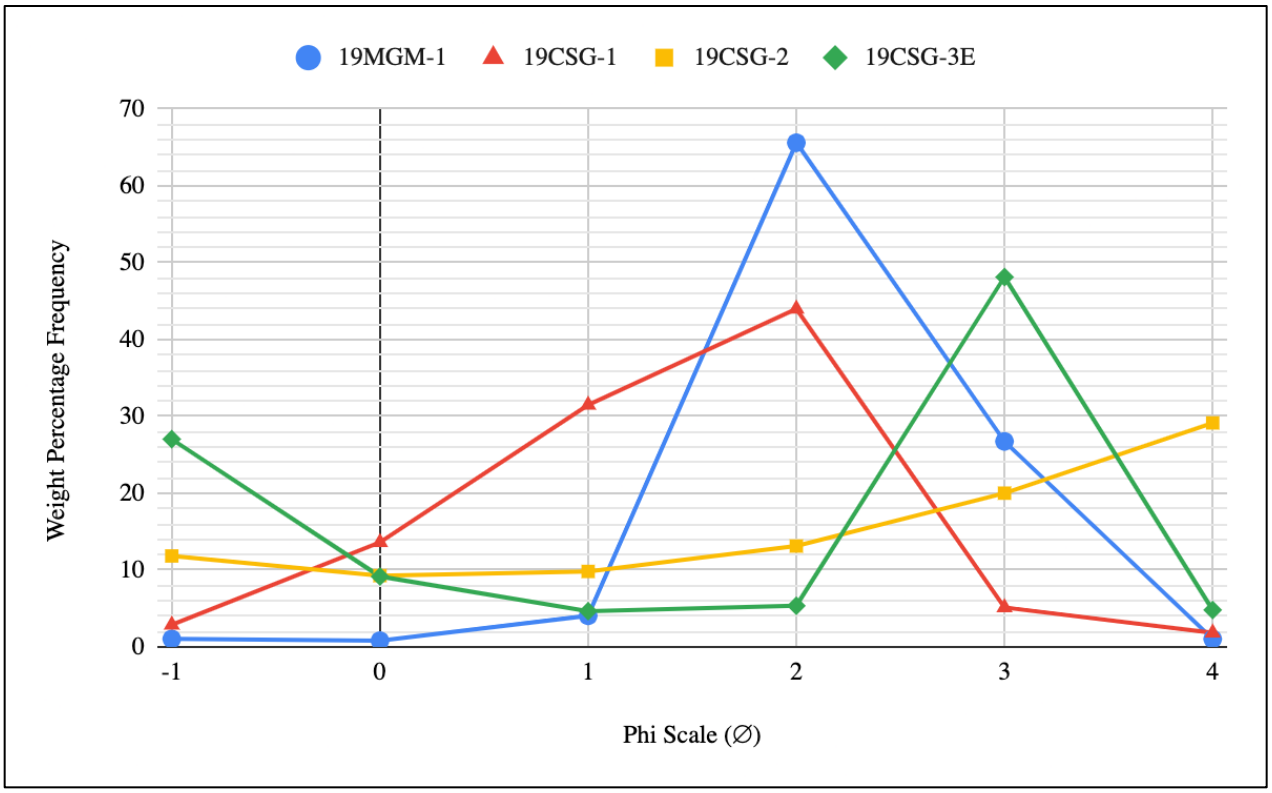

Figure 19. Volume percentage curves of samples from the Eutaw Formation featuring 19MGM-1, 19CSG-1, 19CSG-2, and 19CSG-3E.

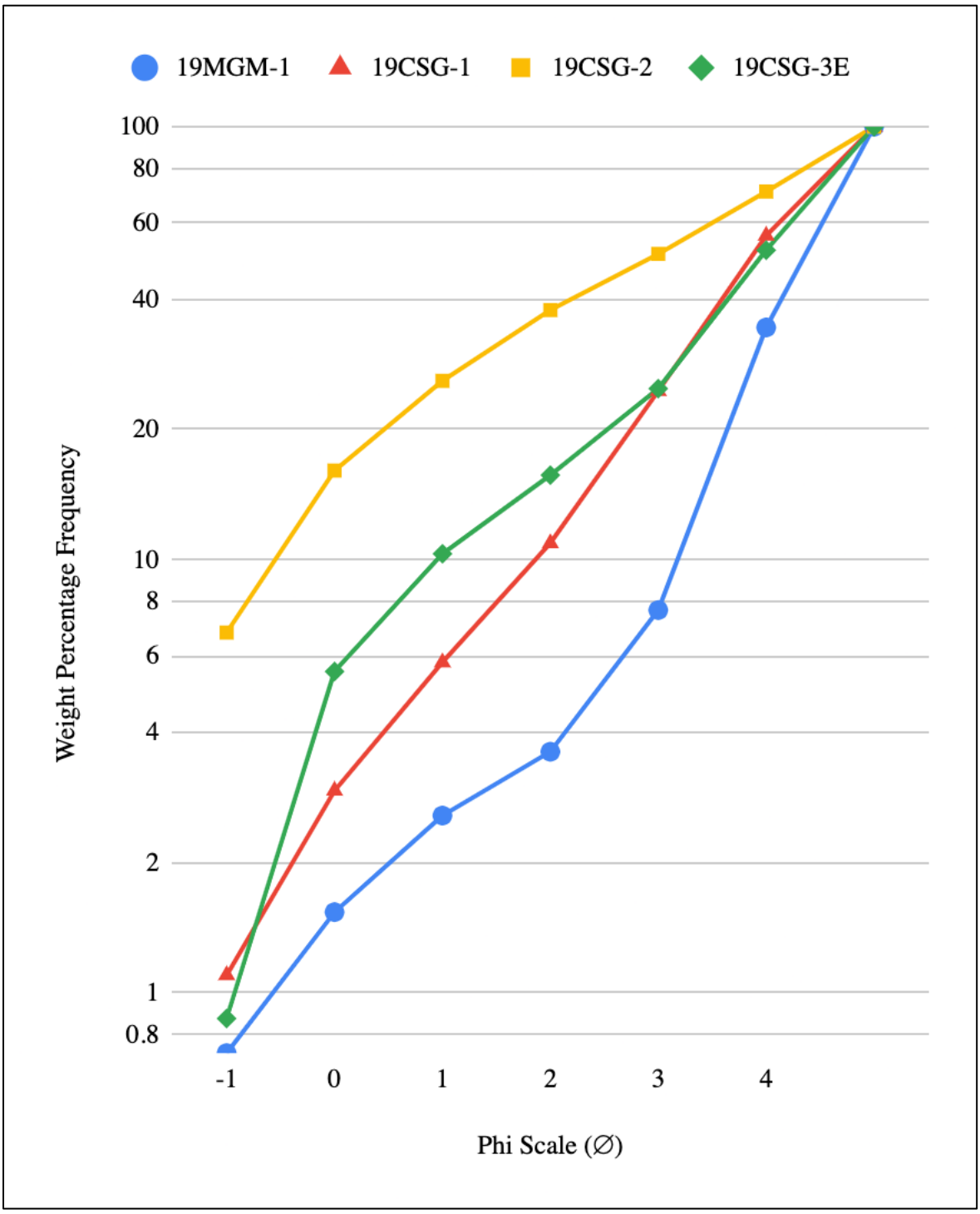

Figure 20. Cumulative curves of samples from the Eutaw Formation.

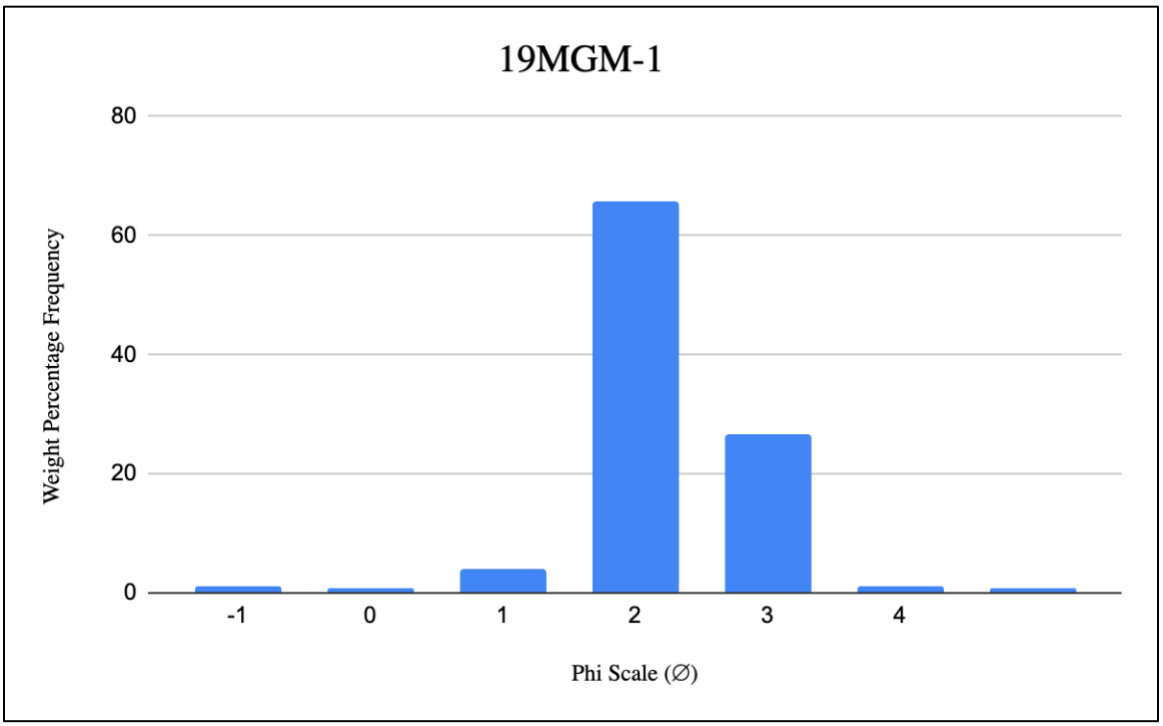

Figure 21. Grain Size Distribution for 19MGM-1

Grain Size (mm)	Phi Scale (Ø)	Wt (g)	Weight Percentage Frequency
2	-1	4.61	1.037456687
1	0	3.6	0.8101614044
0.5	1	17.99	4.048556574
0.25	2	291.53	65.60732062
0.125	3	118.82	26.73982724
0.0625	4	4.58	1.030705342
Pan		3.2259	0.7259721318
		444.3559	

Table 2. Grain Size Distribution Data Analysis for 19MGM-1

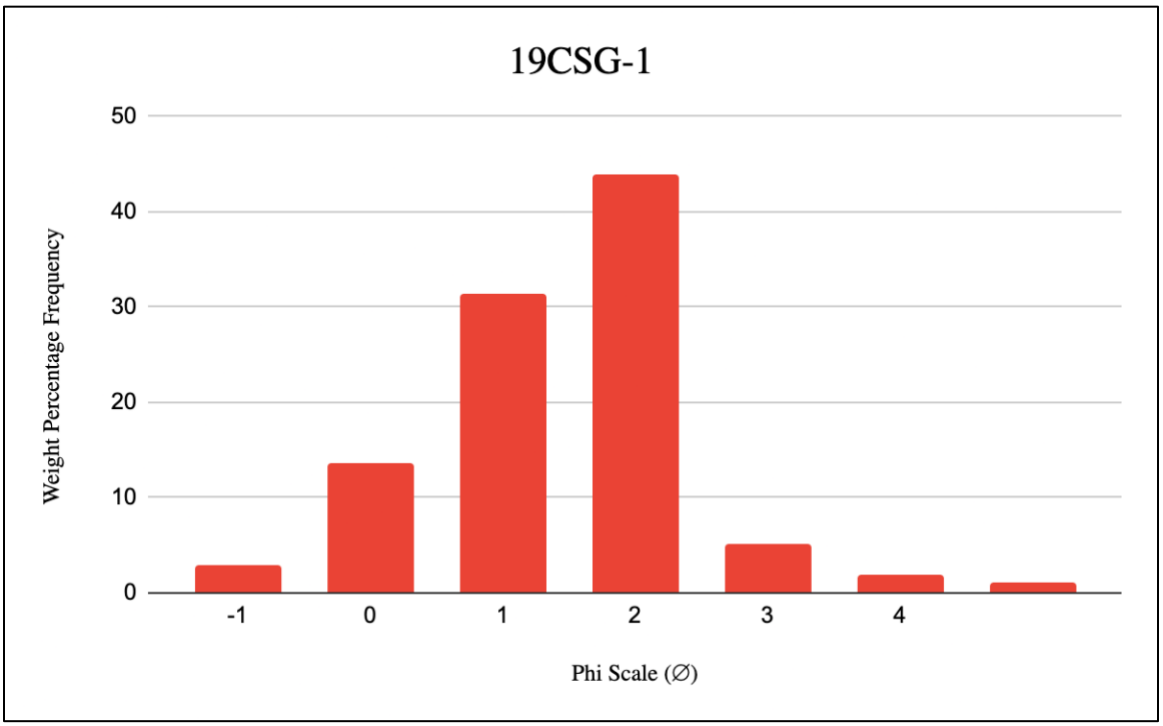

Figure 22. Grain Size Distribution for 19CSG-1

Grain Size (mm)	Phi Scale (Ø)	Wt (g)	Weight Percentage Frequency
2	-1	14.13	2.865965313
1	0	67.09	13.60775746
0.5	1	155.23	31.48505276
0.25	2	216.86	43.98536715
0.125	3	25.27	5.125473706
0.0625	4	9.03	1.831540465
Pan		5.4176	1.098843148
		493.0276	

Table 3. Grain Size Distribution Data Analysis for 19CSG-1

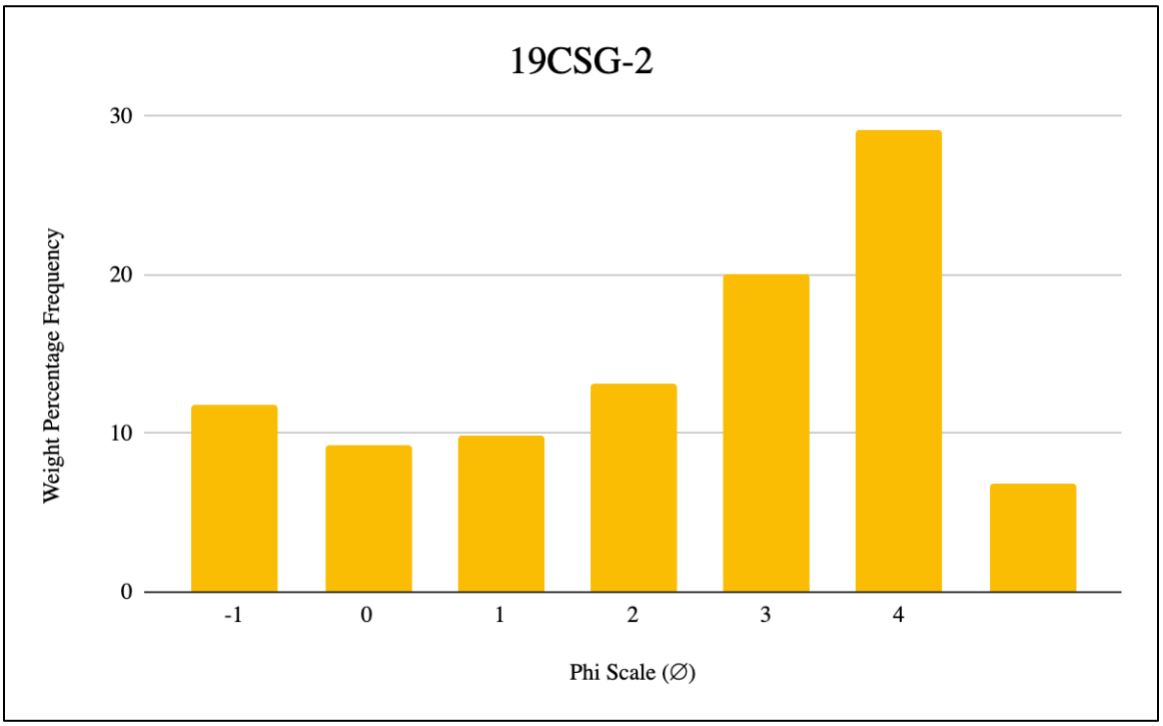

Figure 23. Grain Size Distribution for 19CSG-2

Grain Size (mm)	Phi Scale (Ø)	Wt (g)	Weight Percentage Frequency
2	-1	41.99	11.83250204
1	0	32.93	9.279454448
0.5	1	34.85	9.820497647
0.25	2	46.57	13.12311551
0.125	3	70.99	20.00450869
0.0625	4	103.44	29.14870234
Pan		24.1	6.79121932
		354.87	

Table 4. Grain Size Distribution Data Analysis for 19CSG-2

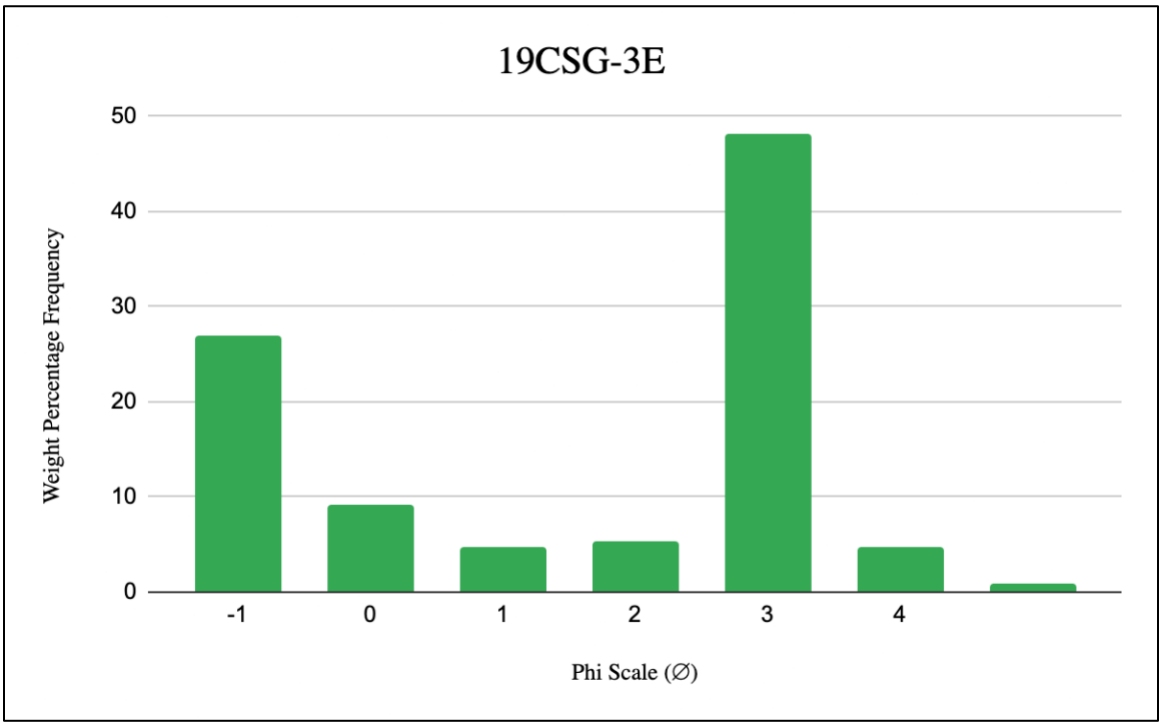

Figure 24. Grain Size Distribution for 19CSG-3E

Grain Size (mm)	Phi Scale (Ø)	Wt (g)	Weight Percentage Frequency
2	-1	109.04	27.03091301
1	0	36.95	9.159870101
0.5	1	18.76	4.650586281
0.25	2	21.61	5.357098589
0.125	3	194.14	48.12712264
0.0625	4	19.37	4.801804705
Pan		3.52	0.8726046754
		403.39	

Table 5. Grain Size Distribution Data Analysis for 19CSG-3E

3.2 Geochemical Results

3.2.1. X-ray Diffraction Results

X-ray diffraction analysis of the samples indicates a mineral suite of a relatively homogeneous nature with high concentrations of quartz. Due to the mineral's abundance and durability in detrital samples, quartz was referenced as the diffraction standard. The Montgomery County sample, 19MGM-1 featured a mineral suite composed of predominantly quartz with accessory minerals making up a minority of the composition (Figure 25). Muscogee County samples, 19CSG-1 (Figure 26), and 19CSG-2 (Figure 27) included a quartz dominated composition. Muscogee County samples feature a similar mineral suite with localized muscovite and accessory mineral assemblages to Russell County sample, 19CSG-3E (Figure 28).

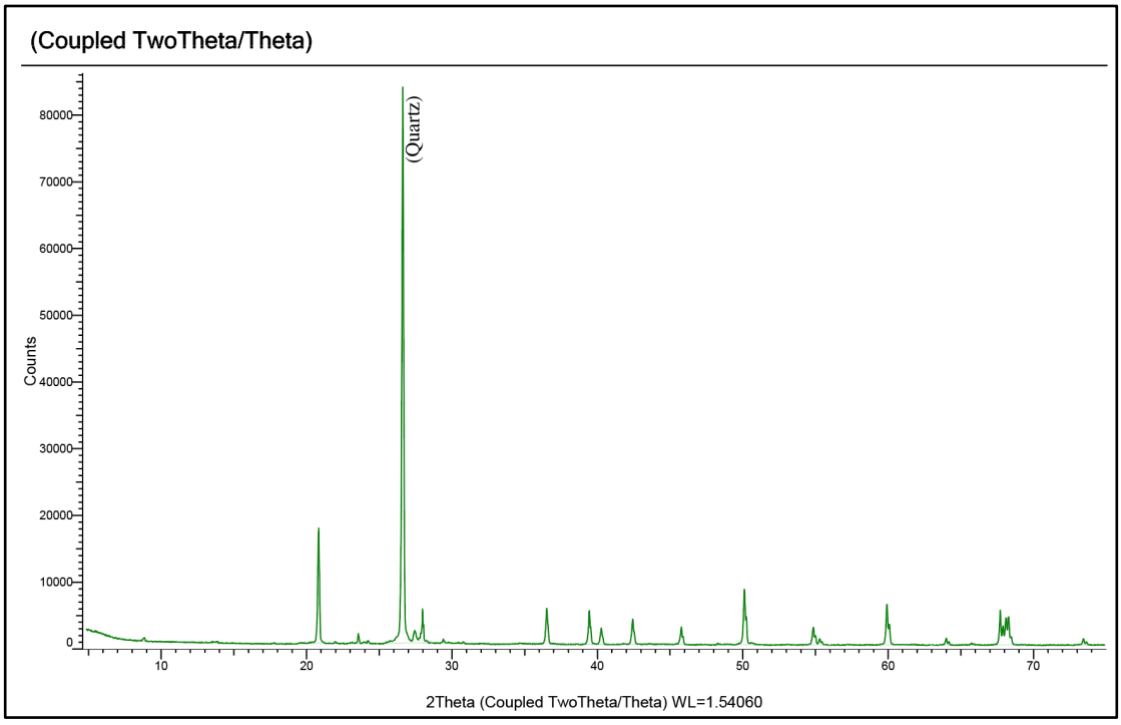

Figure 25. X-ray diffraction peak of 19MGM-1series.

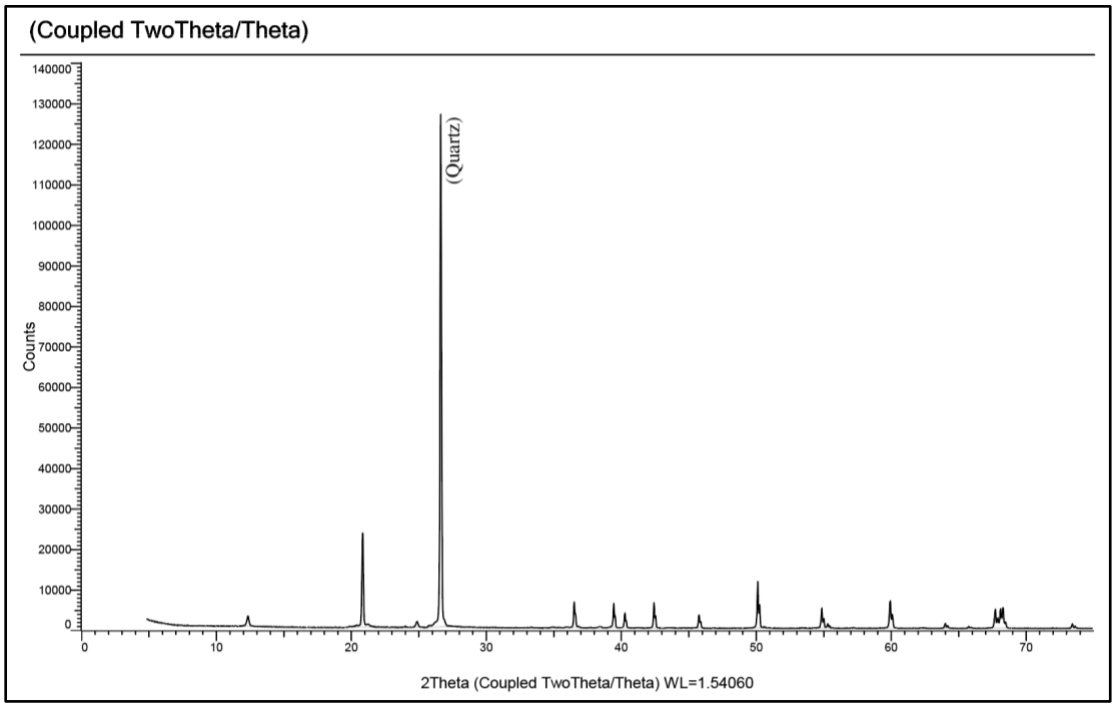

Figure 26. X-ray diffraction peak of 19CSG-1 series.

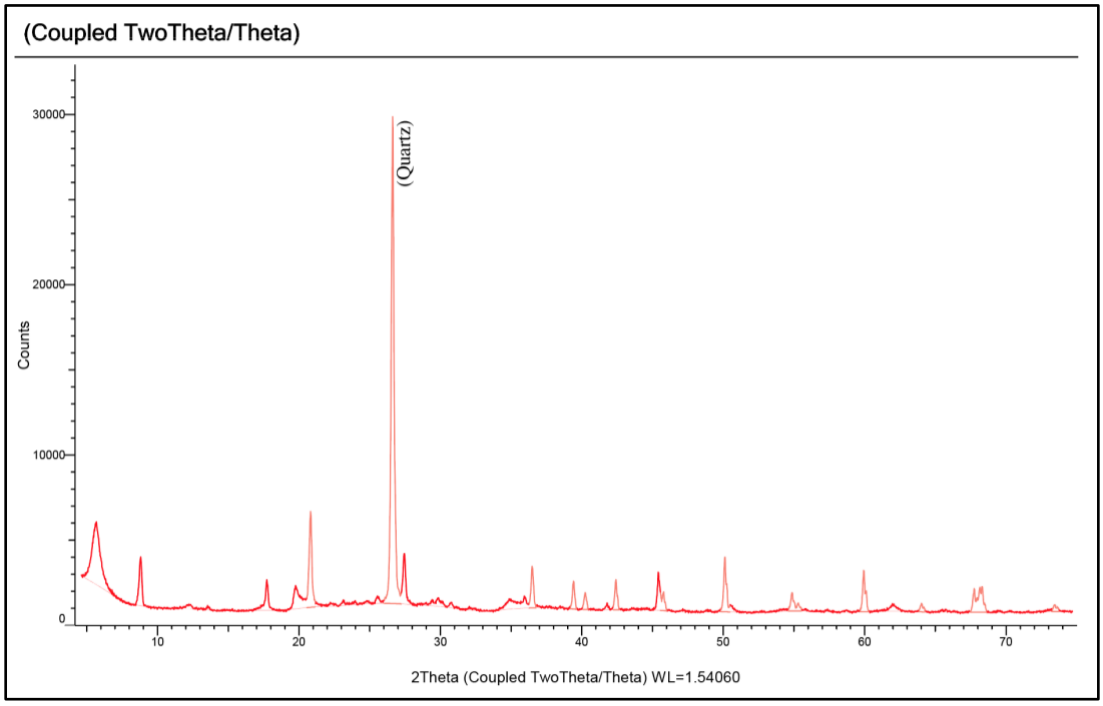

Figure 27. X-ray diffraction peak of 19CSG-2 series.

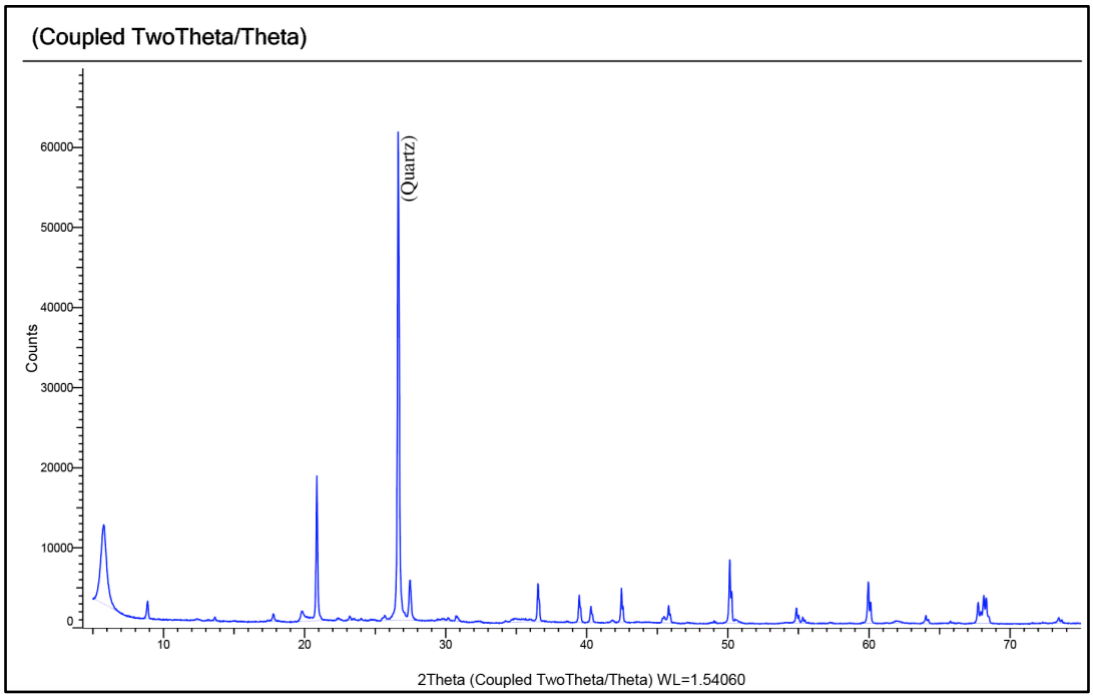

Figure 28. X-ray diffraction peak of 19CSG-3E series.

3.2.2 ICP-AES (Inductively Coupled Plasma Atomic Emission Spectrometry)

Major and trace element concentrations from the whole-rock analysis of 19MGM-1 are provided in Table 6. The overwhelming majority of the Montgomery County sample is SiO_2 with a weight percentage of 93.3%. SiO_2 contents are also highly concentrated in 19CSG-1, 19CSG-2, and 19CSG-3E with weight percentages of 94.5%, 68.4%, 83.2%, respectively.

Table 6. Whole-rock major and trace element concentrations in 19MGM-1.

Major	Wt (%)	Trace	ppm	Trace	ppm
SiO_2	93.3	**Ba**	220	**Pr**	3.83
Al_2O_3	3.08	**Ce**	31.6	**Rb**	22.5
Fe_2O_3	1.15	**Cr**	10	**Sm**	3.32
CaO	0.81	**Cs**	0.37	**Sn**	<1
MgO	0.21	**Dy**	2.45	**Sr**	61.1
Na_2O	0.41	**Er**	1.52	**Ta**	0.3
K_2O	1.01	**Eu**	0.75	**Tb**	0.39
Cr_2O_3	0.002	**Ga**	3.5	**Th**	2.13
TiO_2	0.12	**Gd**	3.02	**Tm**	0.2
MnO	0.02	**Hf**	2.3	**U**	0.82
P_2O_5	0.21	**Ho**	0.48	**V**	15
SrO	<0.01	**La**	14.1	**W**	1
BaO	0.02	**Lu**	0.16	**Y**	13.9
LOI	1.28	**Nb**	2.2	**Yb**	1.34
Total	101.62	**Nd**	15.9	**Zr**	84

Table 7. Whole-rock major and trace element concentrations in 19CSG-1.

Major	Wt (%)	Trace	ppm	Trace	ppm
SiO_2	94.5	**Ba**	16.9	**Pr**	0.38
Al_2O_3	3.64	**Ce**	4.7	**Rb**	1.6
Fe_2O_3	1.66	**Cr**	<10	**Sm**	0.38
CaO	0.03	**Cs**	0.13	**Sn**	<1
MgO	0.02	**Dy**	0.39	**Sr**	3
Na_2O	0.01	**Er**	0.3	**Ta**	0.2
K_2O	0.03	**Eu**	0.04	**Tb**	0.06
Cr_2O_3	0.002	**Ga**	4	**Th**	1.96
TiO_2	0.08	**Gd**	0.41	**Tm**	0.04
MnO	<0.01	**Hf**	2	**U**	0.53
P_2O_5	0.01	**Ho**	0.08	**V**	9
SrO	<0.01	**La**	2.5	**W**	1
BaO	<0.01	**Lu**	0.04	**Y**	2.8
LOI	1.76	**Nb**	1.2	**Yb**	0.36
Total	101.74	**Nd**	1.5	**Zr**	75

Table 8. Whole-rock major and trace element concentrations in 19CSG-2.

Major	Wt (%)	Trace	ppm	Trace	ppm
SiO_2	68.4	**Ba**	577	**Pr**	2.53
Al_2O_3	14.65	**Ce**	21.8	**Rb**	67
Fe_2O_3	1.92	**Cr**	40	**Sm**	2.22
CaO	0.04	**Cs**	1.26	**Sn**	2
MgO	1.25	**Dy**	1.86	**Sr**	55.4
Na_2O	0.12	**Er**	1.41	**Ta**	0.8
K_2O	2.61	**Eu**	0.27	**Tb**	0.27
Cr_2O_3	0.005	**Ga**	17.5	**Th**	4.33
TiO_2	0.52	**Gd**	1.81	**Tm**	0.25
MnO	<0.01	**Hf**	5.6	**U**	1.28
P_2O_5	0.02	**Ho**	0.38	**V**	51
SrO	0.01	**La**	11.1	**W**	1
BaO	0.07	**Lu**	0.18	**Y**	11.1
LOI	10.9	**Nb**	10.7	**Yb**	1.59
Total	100.52	**Nd**	10.6	**Zr**	205

Table 9. Whole-rock major and trace element concentrations in 19CSG-3E.

Major	Wt (%)	Trace	ppm	Trace	ppm
SiO_2	83.2	**Ba**	525	**Pr**	5.08
Al_2O_3	8.06	**Ce**	42.5	**Rb**	49.9
Fe_2O_3	0.73	**Cr**	10	**Sm**	4.41
CaO	0.03	**Cs**	0.65	**Sn**	1
MgO	0.68	**Dy**	6.9	**Sr**	56.3
Na_2O	0.1	**Er**	4.78	**Ta**	0.4
K_2O	2.23	**Eu**	0.59	**Tb**	0.9
Cr_2O_3	<0.002	**Ga**	8	**Th**	8.76
TiO_2	0.3	**Gd**	5.52	**Tm**	0.62
MnO	0.01	**Hf**	7.5	**U**	2.04
P_2O_5	0.01	**Ho**	1.32	**V**	16
SrO	0.01	**La**	20.7	**W**	1
BaO	0.06	**Lu**	0.57	**Y**	46.5
LOI	6.26	**Nb**	5.5	**Yb**	4.35
Total	101.68	**Nd**	19.6	**Zr**	294

3.2.3 ICP-MS (Inductively Coupled Plasma Mass Spectrometry)

The ICP-MS measured a suite of trace elements for each sample. To best enable comparisons with the whole-rock compositions provided from ICP-AES Analysis, the results of ICP-MS are included in the above section. This includes the Montgomery sample, 19MGM-1, as well as Muscogee and Russell County samples as well. Chondrite-normalized REE diagrams for these 4 samples are presented in (Figure 29). All samples are enriched in light rare earth elements and exhibit negative Eu anomalies. REE total contents increase from 19CSG-1 through 19CSG-2 to 19CSG-3. The 3 samples from Muscogee and Russell County display a more pronounced negative Eu anomaly than MGM-1. A primitive-mantle normalized spider diagram is presented in (Figure 30). Ti and K in the spider diagram were calculated from TiO_2 and K_2O, respectively. The peaks of Zr, Ti, and Y in the spider diagram reflect that these elements are immobile high field strength elements. The Zr peak further indicates the presence of zircon [$ZrSiO_4$] in the rock. The peaks of K and Rb are consistent with the presence of glauconite [$(K,Na)(Fe^{3+},Al,Mg)_2(Si,Al)_4O_{10}(OH)_2$] that are enriched in K and Rb.

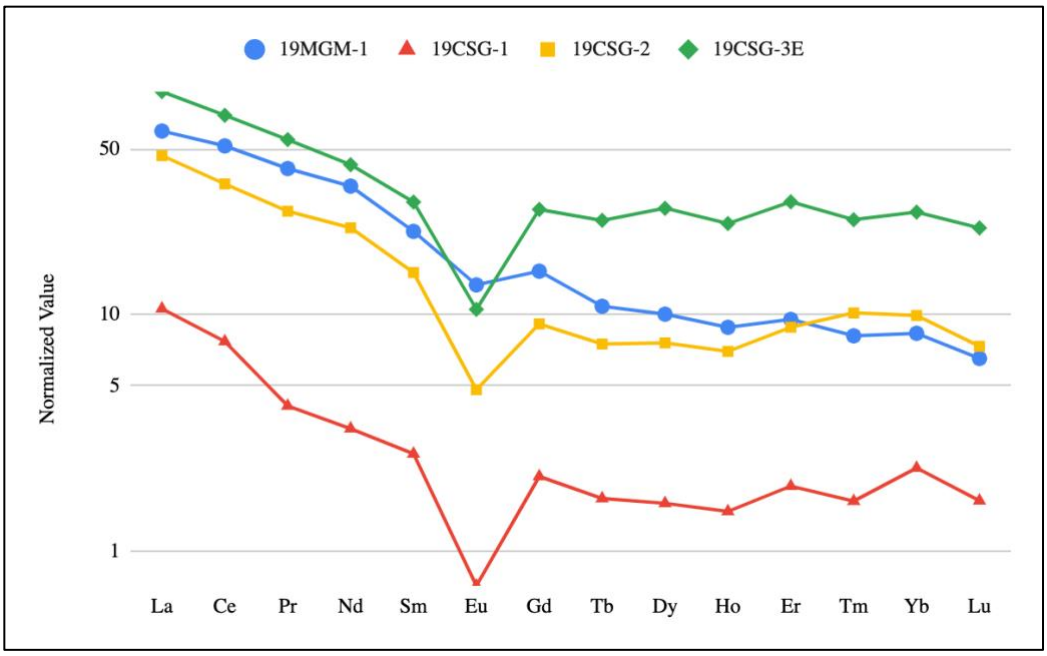

Figure 29. REE patterns for Eutaw Samples. Normalization values of C1 chondrites are from McDonough and Sun (1995).

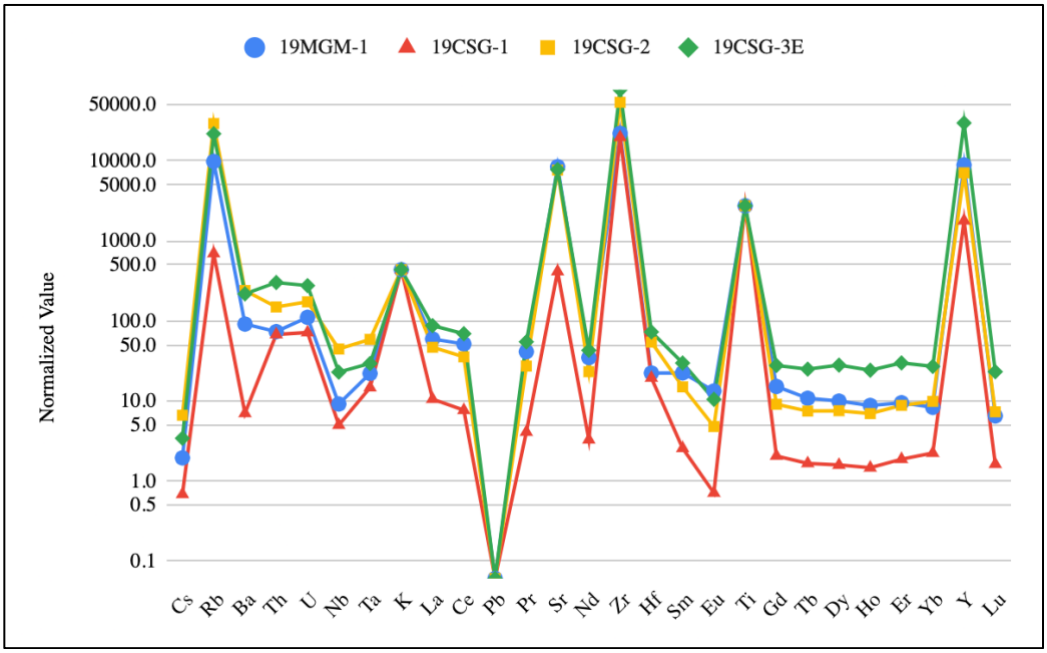

Figure 30. Primitive mantle normalized multi-element plot for Eutaw Samples. Normalization values of primitive mantle are from McDonough and Sun (1995).

3.2.4 Uranium-Lead (U-Pb) Isotopic Dating Results

Uranium-Lead (U-Pb) dating was performed on Lee County sample, 19MGM-1, and Muscogee County sample, 19CSG-1 utilizing SIMS techniques.

SIMS analysis of 19MGM-1 utilized 26 polished zircons (Appendix 1). ^{238}U-^{206}Pb ages of zircons from 19MGM-1 range from 323±11 Ma to 1857±62 Ma (Figure 31). Degrees of discordance range from 0.1% to 10.8%. Using the criterion of 10% discordance for Concordia zircons (Moore et al., 2012), all zircons from 19MGM-1 can be considered concordant. Zircon population versus Age were plotted as histograms for 19MGM-1 (Figure 33) at 50 Ma intervals.

SIMS analysis of 19CSG-1 utilized 40 polished zircons (Appendix 2). ^{238}U-^{206}Pb ages of zircons from 19CSG-1 range from 317±11 Ma to 1307±38 Ma (Figure 32). Except for one grain with a ^{238}U-^{206}Pb age of 651.6 Ma and degree of discordance of 20%, all other 39 zircons have a degree of discordance ranging from 0.5% to 10.6% and can be considered concordant zircons. Zircon population versus age were plotted as histograms for 19CSG-1 (Figure 34) at 50 Ma intervals.

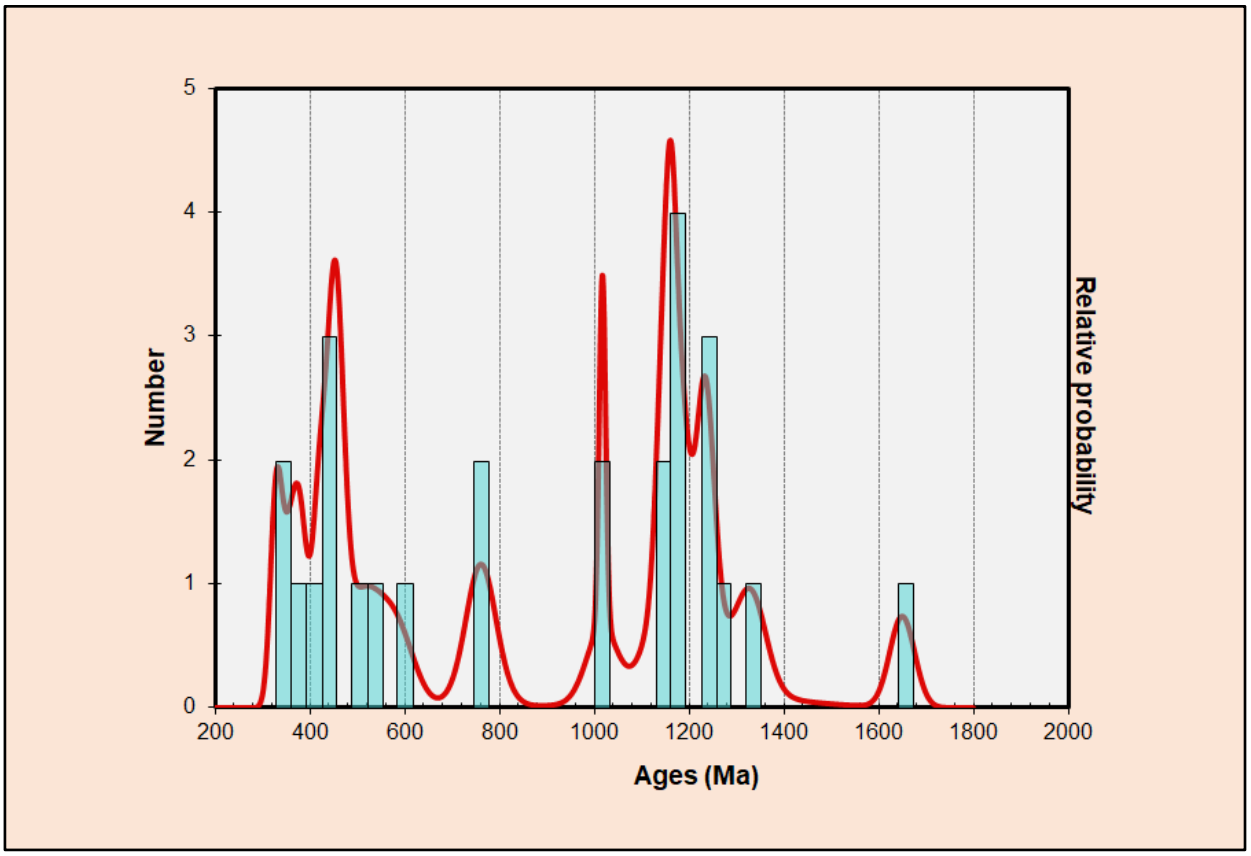

Figure 31. Histogram of Number versus zircon U-Pb ages obtained from 26 zircons in 19MGM-1 measured using SIMS. Note zircon age intervals set at 50 Ma. Relative Probability is plotted as well.

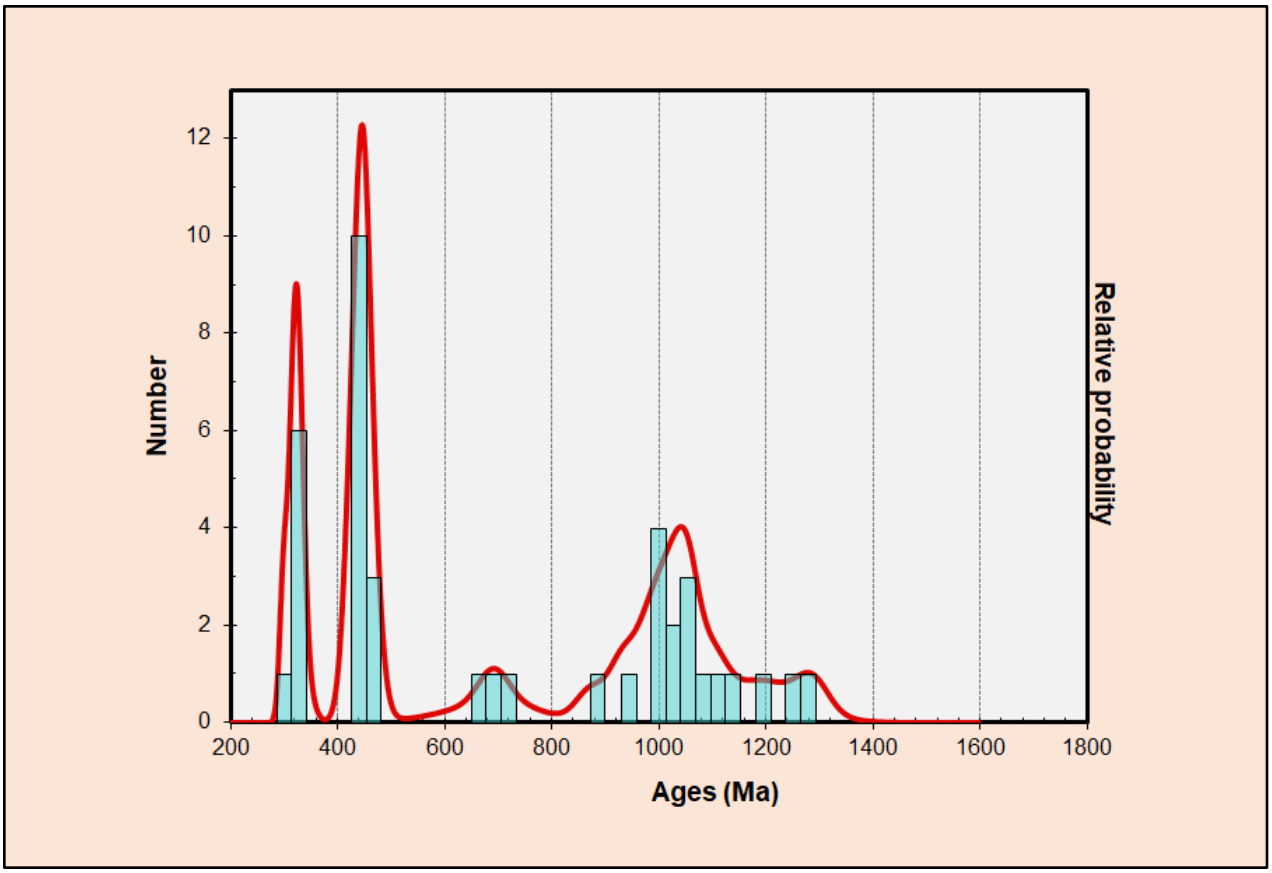

Figure 32. Histogram of Number versus zircon U-Pb ages obtained from 40 zircons in 19CSG-1 measured using SIMS. Note zircon age intervals set at 50 Ma. Relative Probability is plotted as well.

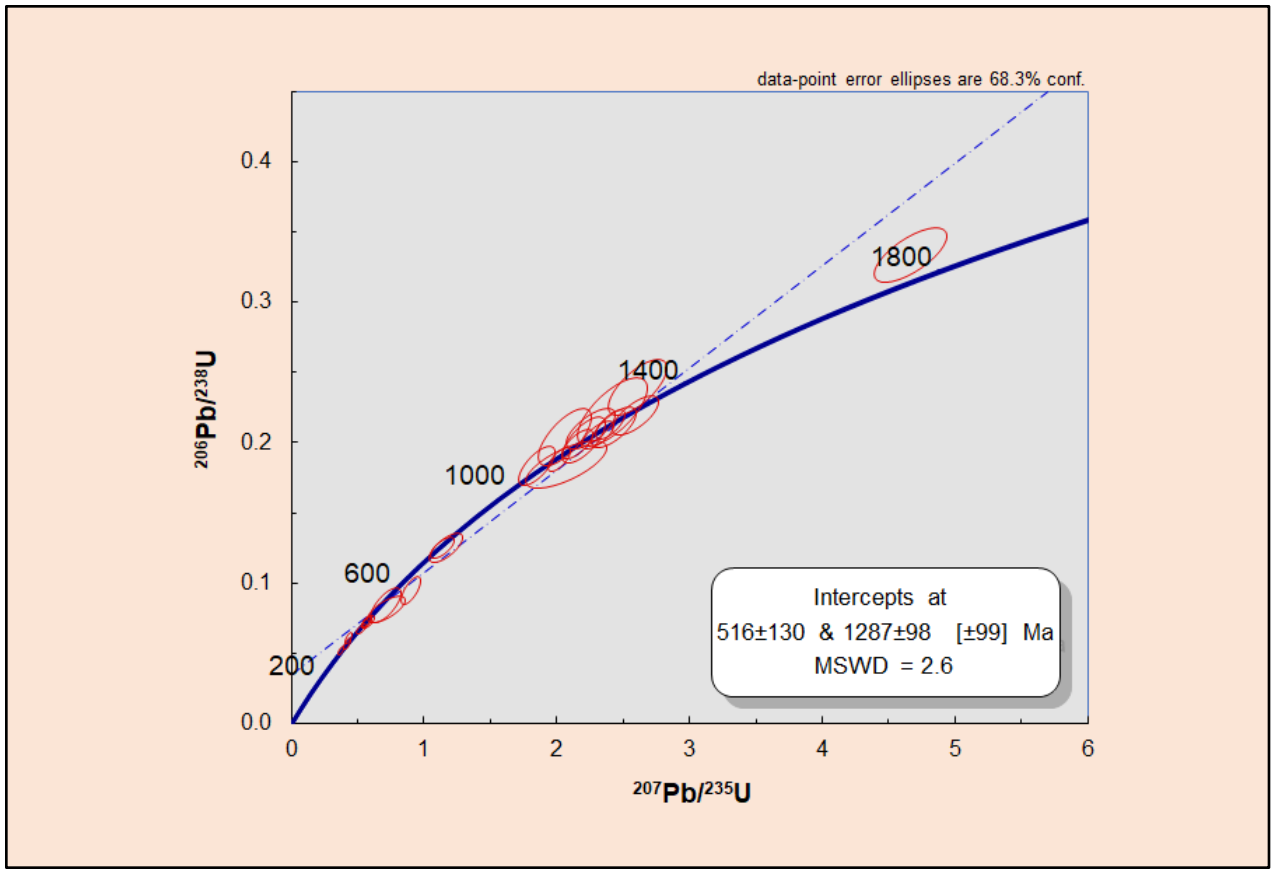

Figure 33. U-Pb Concordia plot of zircon ages obtained from 26 zircons in 19MGM-1 measured using SIMS.

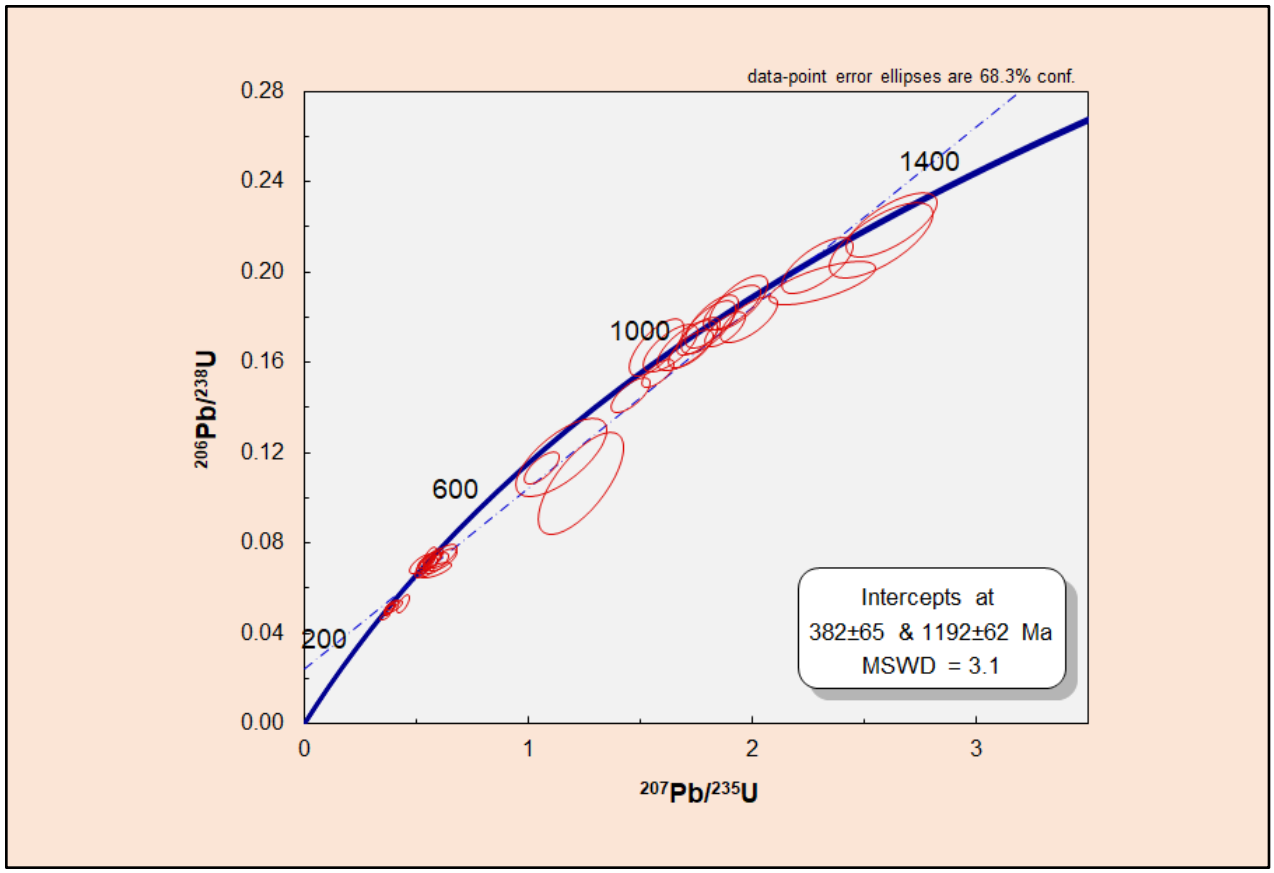

Figure 34. U-Pb Concordia plot of zircon ages obtained from 40 zircons in19CSG-1measured using SIMS.

DISCUSSION

4.1 Zircon Age Populations

4.1.1 Sample 19MGM-1

The age populations from the Montgomery County sample, 19MGM-1, range from 1857±62 Ma to 329±12 Ma. All zircons from 19MGM-1 are concordant and are selected for age population analyses. Of the 26 zircon grains analyzed, 12 (46%) have ages between 950 and 1250 Ma and indicate the importance of the Grenvillian (950 to 1250 Ma) tectonomagmatic event. The Grenville orogeny which was a long-lived Mesoproterozoic mountain-building event associated with the assembly of the supercontinent Rodinia (Tollo et al., 2004). The results of the Grenville orogeny left behind a prominent orogenic belt that spans a significant portion of the North American continent, from Norway to Mexico.

One grain (4%) from 19MGM-1 has an age of 584 +/- 37, indicating Carolina (580 to 640 Ma) tectonomagmatic event. Six (23%) grains have ages between 430 and 500 Ma and indicate Taconian (430 to 500 Ma) tectonomagmatic event. 2 (8%) grains have ages between 350 and 400 Ma and indicate Acadian (350 to 400 Ma) tectonomagmatic event. Only 1 (4%) grain has an age of 329 +/- 12 Ma and indicates Alleghanian (325 to 265 Ma) tectonomagmatic event. In the Appalachians, the Taconic orogeny occurred in the Middle to Late Ordovician, the Acadian orogeny during the Early and Middle Devonian, and the Allegheny orogeny from Middle Mississippian to Middle Permian (DiPietro, 2013, Eriksson et al., 2003, Hatcher, 1989). Between each orogenic event, entire sections of the Appalachians were eroded down to sea level and reclaimed by the sea (Figure 35). Only the last of the orogenic events, the Alleghany/Ouachita orogeny (Melton, 1930), is still preserved.

Two grains (8%) from 19MGM-1 have ages between 760 and 761 Ma and record anorogenic meta-rhyolitic (granitic) igneous activities of 758 +/- 12 Ma (Aleinikoff et al., 1995) associated with the rifting of Rodinia. Two (8%) grains have pre-Grenvillian ages of 1385 and 1857 Ma. It is worth noting that the overall age spectrum for 19MGM-1 is similar to the zircons from Appalachian rivers (Moecher and Samson, 2006).

4.1.2 Sample 19CSG-1

The age populations from the Muscogee County sample, 19CSG-1, range from 1307±37 Ma to 299±7 Ma. Of the 39 Concordia grains that analyzed, 17 (44%) grains have ages between 950 and 1250 Ma and indicate Grenvillian tectonomagmatic event; 13 (33%) grains have ages between 430 and 500 Ma and indicate Taconian (430 to 500 Ma) tectonomagmatic event; 7 (18%) grains have ages between 265-325 Ma and indicate Alleghanian/Ouachita tectonomagmatic event; and 2 grains (5%) have ages of 692 and 718 Ma, indicating anorogenic meta-rhyolitic (granitic) igneous activities associated with the rifting of Rodinia. Grains from Acadian tectonomagmatic events are not detected.

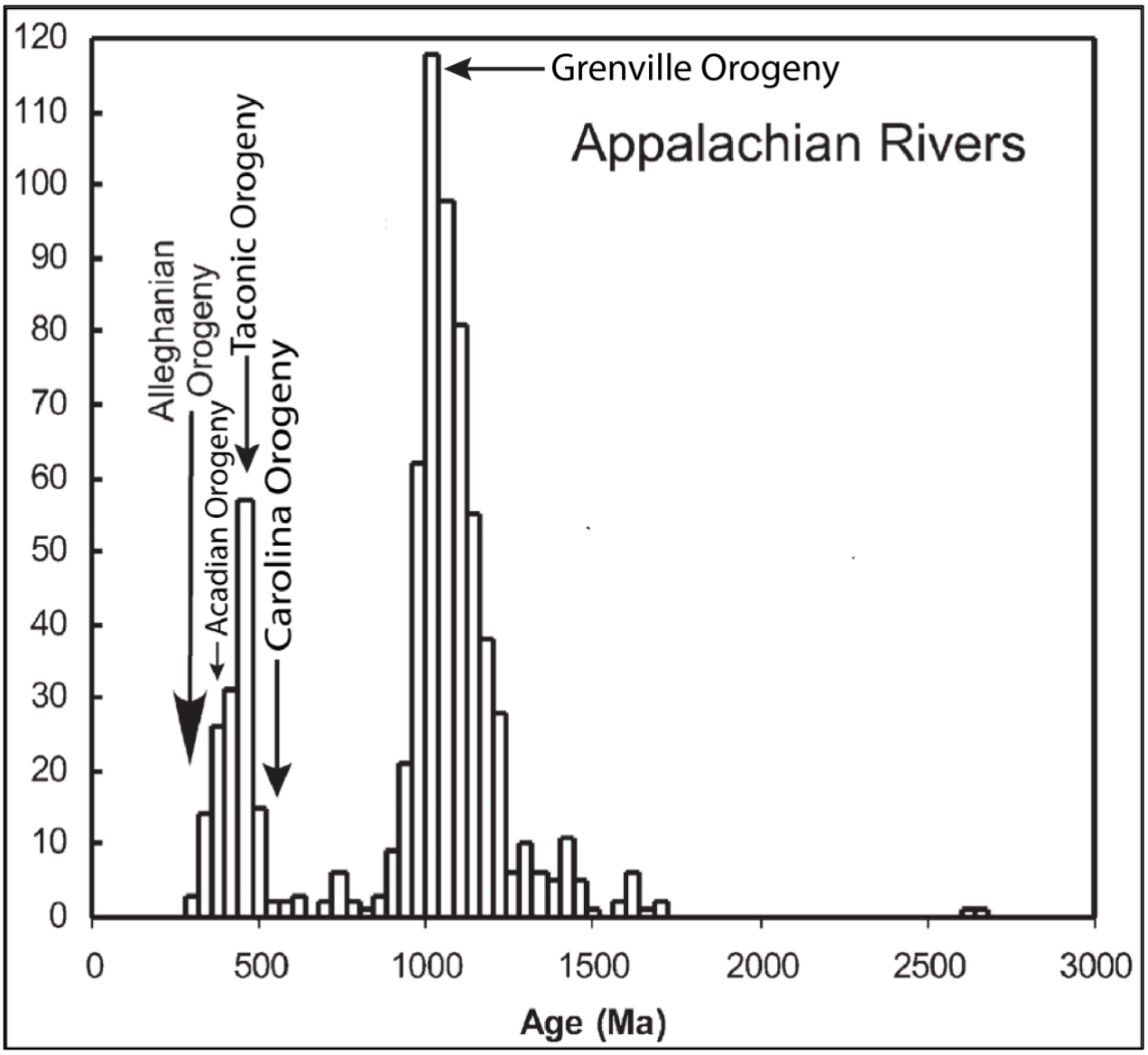

Figure 35. Frequency Distributions for Detrital Age Distributions of Appalachian Rivers (adapted from Moecher and Samson, 2006)

4.1.3 Comparison of 19CSG-1 and 19MGM-1

The proportions of zircons for each tectonomagmatic event are summarized in Table 10. Both 19CSG-1 and 19MGM-1 are similarly dominated by Grenvillian zircons (44% and 46%,

respectively) followed by Taconian zircons (33% and 23%, respectively). But 19CSG-1 has more Alleghanian zircons and less Acadian zircons relative to 19MGM-1. Their overall zircon age distributions are similar to the detrital age distributions of Appalachian rivers (Fig. 35) that are dominated by Grenvillian zircons followed by Taconian zircons, suggesting their origin from the Appalachian mountain.

Table 10. Zircon proportions for each tectonomagmatic event

Sample	Pre-Grenvillian	Grenvillian	Rifting at 700 Ma	Carolina	Taconian	Acadian	Alleghanian
19CSG-1	0%	44%	5%	0%	33%	0%	18%
19MGM-1	8%	46%	8%	4%	23%	8%	4%

4.1.4 Comparison of the youngest detrital zircon age and deposition age

The youngest zircon grain represents the maximum depositional age for clastic sedimentary rocks (Gehrels, 2014). The youngest grain from 19CSG-1 (299 Ma) predates the depositional age for the Eutaw Formation (85 Ma) by 214 Ma; the youngest grain from 19MGM-1 (329 Ma) predates the depositional age for the Eutaw Formation (85 Ma) by 244 Ma.

4.2 Implications of Clastic Detritus Transportation

Clastic Detritus in the Gulf Coast region is heavily influenced by coastal events throughout geologic time. During Late Cretaceous, this included transgressive oscillations, storm-driven climate, and increased modes of detrital transportation such as the western interior seaway. The Gulf Coastal Boundary, in particular, underwent a series of transgressive oscillations during

Late Cretaceous increasing the probability of sediment transportation along the coastline (Hancock and Kauffman, 1979). Much of the boundary has been exposed at various points throughout geologic history, including the depositional period of the Eutaw Formation. Clastic detritus affected by transgressive oscillation during the Cretaceous would have been susceptible to longshore drift as a mechanism for sediment dispersal along the Gulf Coastal Plain Boundary. Southeasterly paleowind directions of Late Cretaceous would have influenced longshore drift along the Upper Cretaceous coastal plain boundary (Elder, 1988).

The Chattahoochee Valley locality of 19CSG-1 was a known estuarine area during Late Cretaceous fed by the Chattahoochee river system (Schwimmer, 2002). Much of the zircon populations associated with 19CSG-1 are indicative of Appalachian orogenic events likely fed by this river system. Detrital zircons following the southwestern paleocurrents of the Appalachian sediments through the Chattahoochee Valley would have contributed to longshore drift during the transgressive episodes of Late Cretaceous. This may account for the age populations seen in 19MGM-1, a sample over 100 miles west of the Chattahoochee valley locality, and yet heavily influenced by Appalachian orogenic events.

Deposition of the Eutaw Formation was influenced by more than just longshore drift, however. The Upper Cretaceous coastal plain boundary was influenced by coastal and geographical conditions as well. Late Cretaceous was known for its severe and disruptive climatic conditions experiencing an increase in storm activity due to increased temperatures and humidity levels (Hallam, 1984). There is evidence to suggest a North American monsoon during the time of deposition for the Eutaw Formation (Allen, 1975). Additionally, the Upper Cretaceous coastal plain boundary was connected to the western interior seaway and was likely influenced by the storm-driven, shore-parallel shelf currents found during this period (Ericksen and Slingerland,

1990). The zircon age distributions from 19CSG-1 and 19MGM-1 dominated by the Grenville zircons and Taconic zircons indicate the main influence by the Chattahoochee River system being fed by Appalachian detritus. The lack of zircons younger than Alleghanian suggests that the western interior seaway magmatic rocks were not a major source for the Eutaw Formation at Columbus and Montgomery.

4.3 Source rock lithology from geochemical composition

Geochemical data of sandstone may reflect the durability of individual grains. Clastic detrital samples such as the samples utilized in this experiment are generally old enough to have undergone several phases of physical and/or chemical weathering during transportation from source rock. X-ray diffraction analysis of the samples indicates a mineral suite of a relatively homogeneous nature with high concentrations of quartz, a highly durable mineral commonly found in detrital samples due to its increased resistance to weathering. Quartz dominated composition suggest pronounced chemical weathering and increased sediment transport from source lithology. All samples referenced quartz as the diffraction standard due to its relative abundance and durability in detrital sediments. While dominated by quartz composition, durable accessory minerals make up an insignificant minority of overall composition including but not limited to the accessory mineral, zircon. Durable minerals such as quartz and zircon, reflect upon the age and transportation of sediments included in the Eutaw Formation likely having been included in the source rock lithology and are verified in the age population distributions of samples, 19MGM-1 and 19CSG-1. All samples are enriched in light rare earth elements and exhibit negative Eu anomalies. REE total contents increase from 19CSG-1 through 19CSG-2 to 19CSG-3. The 3 samples from Muscogee and Russell County areas display a more pronounced

negative Eu anomaly than MGM-1. Europium depletion in samples reflects magma solidification isolated from Eu enriched plagioclase for each sample. Sample 19MGM-1 is slightly less depleted of Europium than other samples suggesting that a small amount of Eu-enriched plagioclase crystals might have survived the transportation and are present in 19MGM-1.

4.4 Implications of grain-size distribution on sediment transport and deposition

Grain-Size analysis of all samples revealed much about sediment mode of transportation and depositional settings. Whole-rock analysis of sediments revealed a quartz dominated composition of all samples to varying SiO_2 weight percentages; 19MGM-1 (93.3%), 19CSG-1 (94.5%), 19CSG-2 (68.4%), 19CSG-3E (83.2%). Quartz durability suggests increased sediment transport. Grain shape analysis indicated subrounded to rounded textures for samples 19CSG-1, 19CSG-2, and 19CSG-3E. Grain shape analysis indicated subangular to rounded textures for sample, 19MGM-1 The increased angularity of 19MGM-1 supports the theory of longshore drift following the southeasterly paleowind direction of Late Cretaceous (Elder 1988) by exhibiting a well-rounded grain size distribution when plotted as histograms (Figure 21-24). Grain sorting of this nature further confirms longer sediment transportation from source rock as grain sorting tends to occur over the increased spatial difference from source to deposition. Given the presence of the Chattahoochee estuarine area during the depositional period, fluvial transportation of clastic sediments likely followed the southwestern paleocurrents of the Appalachian sediments.

CONCLUSIONS

1. The overall zircon age distributions for samples 19MGM-1 and 19CSG-1 are dominated by Grenvillian zircons (44-46%) followed by Taconian zircons (23-33%) with minor Acadian and Alleghanian zircons. Their age distributions are similar to the detrital age distributions of Appalachian rivers, suggesting their origin from the Appalachian orogen. The lack of zircon age peaks at greater than 1.8 Ga indicates that Ouachitas were not a significant source for the sandstones in this study.
2. Geochemical (ICP-MS and ICP-AES) and grain-size analysis revealed a well-sorted, quartz dominated sediment composition included in the Eutaw Formation, confirming increased sediment transportation from the source. This increases the likelihood of having been included in the source rock lithology suggested in zircon age populations. Susceptible to transgressive oscillations during deposition, detrital zircons likely followed the southwestern paleocurrents of the Chattahoochee river system. Appalachian sediments were likely transported along the coastal plain boundary as witnessed in the zircon age distributions of Montgomery County sample, 19MGM-1.
3. The results of this study suggest greater sediment influx from older (Grenville dominated) upper-continental source terrane in the eastern United States. Provenance investigation through geochemical and grain-size analysis of the Eutaw Formation has helped to further constrain our depositional understanding of eastern Alabama and western Georgia along the Upper Cretaceous coastal plain boundary. Sandstone provenance of the Eutaw Formation is a mix of eastern United States orogenic events.

REFERENCES

1.5: ICP-AES Analysis of Nanoparticles - Chemistry LibreTexts, https://chem.libretexts.org/Bookshelves/Analytical_Chemistry/Book%3A_Physical_Methods_in_Chemistry_and_Nano_Science_(Barron)/01%3A_Elemental_Analysis/1.05%3A_ICP-AES_Analysis_of_Nanoparticles (accessed February 2020).

1.6: ICP-MS for Trace Metal Analysis - Chemistry LibreTexts, https://chem.libretexts.org/Bookshelves/Analytical_Chemistry/Book%3A_Physical_Methods_in_Chemistry_and_Nano_Science_(Barron)/01%3A_Elemental_Analysis/1.06%3A_ICP-MS_for_Trace_Metal_Analysis (accessed February 2020).

Aleinikoff, J.N., Zartman, R.E., Walter, M., Rankin, D.W., Lyttle, P.T., and Burton, W.C., 1995, U-Pb ages of metarhyolites of the Catoctin and Mount Rogers formations, central and southern Appalachians: evidence for two pulses of Iapetan rifting: American Journal of Science, v. 295, p. 428–454, http://pubs.er.usgs.gov/publication/70019090.

Allen, P., 1975, Wealden of the Weald: a new model: Proceedings of the Geologists' Association, v. 86, p. 389–437, doi:10.1016/S0016-7878(75)80057-5.

Black, D.L., Barineau, C.I., and Frazier, W.J., 2015, Paleorelief of the coastal plain unconformity of southwestern Georgia: Evidence for a long-lived Cretaceous paleodrainage system: Southeastern Geological Society Guidebook, v. 65, p. 15–34, https://segs.org/wp-content/uploads/2010/01/SEGS-Guidebook-65-2015.pdf.

Britton, T.A., 1968, Depositional Environment of the Tombigbee Sand Member-Mooreville Formation Contact at Selected Outcrops in Alabama.:

Butler, J.R., and Ragland, P.C., 1969, Petrology and chemistry of meta-igneous rocks in the Albemarle area, North Carolina slate belt: American Journal of Science, v. 267, p. 700–726,

doi:10.2475/ajs.267.6.700.

Chiarenzelli, J., Lupulescu, M., Cousens, B., Thern, E., Coffin, L., and Regan, S., 2010, Enriched Grenvillian lithospheric mantle as a consequence of long-lived subduction beneath Laurentia: Geology, v. 38, p. 151–154, doi:10.1130/G30342.1.

Cooper, K., 2016, Ion Probe Dating Of Zircon Xenocrysts From Wuluke Volcano, Northwestern Tiber, China: Constraints On Magma Evolution And Deep Crustal Evolution: Auburn University, 79 p., doi:10.1130/abs/2016se-273437.

Dalrymple, G., 1994, The age of the Earth: Stanford University Press, https://books.google.com/books?hl=en&lr=&id=a7S3zaLBrkgC&oi=fnd&pg=PA1&dq=the+age+of+the+earth+dalrymple&ots=ZbDkTZfZ2x&sig=pT7QDd3w3vo1nSmZWO8drT6yx8U (accessed January 2020).

David T. King, J., 1990, Facies Stratigraphy and Relative Sea-Level History--Upper Cretaceous Eutaw Formation, Central and Eastern Alabama: ABSTRACT: AAPG Bulletin, v. 74, doi:10.1306/20b23129-170d-11d7-8645000102c1865d.

Davis, M.E., 1988, Stratigraphic and hydrogeologic framework of the Alabama coastal plain:, doi:10.3133/wri874112.

Dennis, A.J., and Wright, J.E., 1997, The Carolina terrane in northwestern South Carolina, U.S.A.: Late Precambrian-Cambrian deformation and metamorphism in a peri-Gondwanan oceanic arc: Tectonics, v. 16, p. 460–473, doi:10.1029/97TC00449.

DiPietro, J.A., 2013, Tectonic Style, Rock Successions, and Tectonic Provinces, *in* Landscape Evolution in the United States, Elsevier, p. 345–363, doi:10.1016/b978-0-12-397799-1.00021-x.

Dobie, J.L., 1978, A fossil amniote egg from an Upper Cretaceous deposit (Mooreville Chalk of

the Selma Group) in Alabama: Copeia, v. 1978, p. 460, doi:10.2307/1443612.

Ebersole, J., 2013, A Note of Late Cretaceous Fish Taxa Recovered from Stream Gravels at Site AGr-43 in Greene County, Alabama: v. 31, p. 84–97.

Elder, W.P., 1988, Geometry of Upper Cretaceous bentonite beds: implications about volcanic source areas and paleowind patterns, western interior, United States: Geology, v. 16, p. 835–838, doi:10.1130/0091-7613(1988)016<0835:GOUCBB>2.3.CO;2.

Ericksen, M.C., and Slingerland, R., 1990, Numerical simulations of tidal and wind-driven circulation in the Cretaceous Interior Seaway of North America: Geological Society of America Bulletin, v. 102, p. 1499–1516, doi:10.1130/0016-7606(1990)102<1499:NSOTAW>2.3.CO;2.

Eriksson, K.A., Campbell, I.H., Palin, J.M., and Allen, C.M., 2003, Predominance of Grenvillian magmatism recorded in detrital zircons from modern Appalachian rivers: Journal of Geology, v. 111, p. 707–717, doi:10.1086/378338.

Ettensohn, F.R., 1987, Rates of Relative Plate Motion During the Acadian Orogeny Based on the Spatial Distribution of Black Shales: The Journal of Geology, v. 95, p. 572–582, doi:10.1086/629150.

Farías, S., and Smichowski, P., 1999, Determination of germanium at trace levels in environmental matrices by chloride generation-inductively coupled plasma atomic emission spectrometry: Journal of analytical atomic spectrometry, v. 14, p. 809–814, doi:10.1039/a808981g.

Finch, R.J., and Hanchar, J.M., 2018, Structure and chemistry of zircon and zircon-group minerals, *in* Zircon, De Gruyter Mouton, v. 53, p. 1–26, doi:10.2113/0530001.

Frazier, W.J., 1982, Sedimentology and paleoenvironmental analysis of the Upper Cretaceous

Tuscaloosa and Eutaw Formations in western Georgia: Second Symposium on Geology of the Southeastern Coastal Plain, p. 39–52.

Gehrels, G., 2014, Detrital Zircon U-Pb Geochronology Applied to Tectonics: Annual Review of Earth and Planetary Sciences, v. 42, p. 127–149, doi:10.1146/annurev-earth-050212-124012.

Gilstrap, R.A., 2009, A Colloidal Nanoparticle Form of Indium Tin Oxide: System Development and Characterization: Georgia Institute of Technology.

Grove, M., Bebout, G.E., Jacobson, C.E., Barth, A.P., Kimbrough, D.L., King, R.L., Zou, H., Lovera, O.M., Mahoney, B.J., and Gehrels, G.E., 2008, The Catalina Schist: Evidence for middle Cretaceous subduction erosion of southwestern North America: Special Paper of the Geological Society of America, v. 436, p. 335–361, doi:10.1130/2008.2436(15).

Hallam, A., 1984, Continental humid and arid zones during the jurassic and cretaceous: Palaeogeography, Palaeoclimatology, Palaeoecology, v. 47, p. 195–223, doi:10.1016/0031-0182(84)90094-4.

Hancock, J.M., and Kauffman, E.G., 1979, The great transgressions of the Late Cretaceous: Journal of the Geological Society, v. 136, p. 175–186, doi:10.1144/gsjgs.136.2.0175.

Hatcher Jr., R.D., Thomas, W.A., and Viele, G.W., 1989, The Appalachian-Ouachita Orogen in the United States: Geological Society of America, 768 p., doi:10.1130/DNAG-GNA-F2.

Hibbard, J.P., Stoddard, E.F., Secor, D.T., and Dennis, A.J., 2002, The Carolina zone: Overview of neoproterozoic to early paleozoic peri-gondwanan terranes along the eastern flank of the southern Appalachians: Earth-Science Reviews, v. 57, p. 299–339, doi:10.1016/S0012-8252(01)00079-4.

Holland, S.M., and Patzkowsky, M.E., 1997, Distal Orogenic Effects on Peripheral Bulge Sedimentation: Middle and Upper Ordovician of the Nashville Dome: SEPM Journal of

Sedimentary Research, v. Vol. 67, p. 250–263, doi:10.1306/d4268545-2b26-11d7-8648000102c1865d.

Hooper, R.J., and Hatcher, R.D., 1988, Pine Mountain terrane, a complex window in the Georgia and Alabama Piedmont; evidence from the eastern termination: Geology, v. 16, p. 307–310, doi:10.1130/0091-7613(1988)016<0307:pmtacw>2.3.co;2.

Indares, A., Rivers, T., Indares, A., and Rivers, T., 1995, Textures, metamorphic reactions and thermobarometry of eclogitized metagabbros: a Proterozoic example;Textures, metamorphic reactions and thermobarometry of eclogitized metagabbros: a Proterozoic example: EJMin, v. 7, p. 43–56, doi:10.1127/EJM/7/1/0043.

Ingle, S., Mueller, P.A., Heatherington, A.L., and Kozuch, M., 2003, Isotopic evidence for the magmatic and tectonic histories of the Carolina terrane: Implications for stratigraphy and terrane affiliation: Tectonophysics, v. 371, p. 187–211, doi:10.1016/S0040-1951(03)00228-2.

Instrumentation, 2017, https://www.geow.uni-heidelberg.de/HIP/instrumentation_en.html (accessed February 2020).

Ireland, T.R., and Williams. I. S., 2003, Considerations in Zircon Geochronology by SIMS: Reviews in Mineralogy and Geochemistry, doi:10.2113/0530215.

Jones, D., 1967, Geology of the coastal plain of Alabama: New Orleans, Louisiana, Alabama Geological Society.

King, D., 2003, In memoriam - with reference included: Geological Society of America, Sedimentary Geology Division Newsletter, v. 17, p. 8.

King, D., Zou, H.B., Gill, K.K., Petruny, L. W., Smith, F., 2019, Detrital zircons from the Margaret Creek Formation, Corozal Basin, Northern Belize. GeoGulf Transactions, v. 69, p.

221-231.

Košler, J., and Sylvester, P.J., 2013, Present trends and the future of zircon in geochronology: Laser ablation ICPMS: Zircon, v. 53, p. 243–275, doi:10.2113/0530243.

Mancini, E.A., and Tew, B.H., 1993, Eustasy versus subsidence: Lower Paleocene depositional sequences from southern Alabama, eastern Gulf Coastal Plain: Geological Society of America Bulletin, v. 105, p. 3–17, doi:10.1130/0016-7606(1993)105<0003:EVSLPD>2.3.CO;2.

McDonough, W.F., and Sun, S. s., 1995, The composition of the Earth: Chemical Geology, v. 120, p. 223–253, doi:10.1016/0009-2541(94)00140-4.

McKeegan, K. IMS-1290:, https://sims.ess.ucla.edu/nsf_facility/ims1270.php.

Melton, F.A., 1930, Age Of The Ouachita Orogeny and its Tectonic Effects: AAPG Bulletin , v. 14, p. 57–72, https://pubs.geoscienceworld.org/aapgbull/article-pdf/14/1/57/4348970/aapg_1930_0014_0001_0057.pdf (accessed February 2020).

Moecher, D.P., and Samson, S.D., 2006, Differential zircon fertility of source terranes and natural bias in the detrital zircon record: Implications for sedimentary provenance analysis: Earth and Planetary Science Letters, v. 247, p. 252–266, doi:10.1016/j.epsl.2006.04.035.

Monroe, W.H., and Stephenson, L.W., 1938, Stratigraphy of Upper Cretaceous series in Mississippi and Alabama: AAPG Bulletin, v. 22, p. 1639–1657, http://archives.datapages.com/data/bulletns/1938-43/data/pg/0022/0012/1600/1639.htm (accessed June 2019).

Moore, J.M., Polteau, S., Armstrong, R.A., Corfu, F., and Tsikos, H., 2012, The age and correlation of the Postmasburg Group, southern Africa: Constraints from detrital zircon grains: Journal of African Earth Sciences, v. 64, p. 9–19,

doi:10.1016/j.jafrearsci.2011.11.001.

NYC Regional Geology, https://web.archive.org/web/20110722153634/http://3dparks.wr.usgs.gov/nyc/highlands/highlands.html (accessed April 2020).

of Alabama, S., 2005, Final Catoma Creek TMDL Catoma Creek Watershed in the Alabama River Basin.:

Osborne, D., 2013, Provenance of detrital sand of the Eutaw Formation in Alabama and western Georgia: Implications for Late Cretaceous paleogeography: Columbus State University, 34 p., http://csuepress.columbusstate.edu/abstracts.

Reinhardt, B.J., Schindler, J.S., Gibson, T.G., Smith, C.C., Sohl, N.F., Edwards, L.E., and Laurel, M., 1994, Geologic Map Of The Americus 30 ' x 60 ' Quadrangle, Georgia And Alabama: , p. 1–8.

Russell, E.E., and Keady, D.M., 1990, Geologic mapping of Upper Cretaceous units in northeastern Mississippi: Mississippi Office of Geology Circular, p. 15–16.

Ryder, R.T., Swezey, C.S., Crangle, R.D., and Trippi, M.H., 2008, Geologic Cross Section E-E' Through the Appalachian Basin From the Findlay Arch, Wood County Ohio, to The Valley and Ridge Province, Pendleton County, West Virginia, *in* U.S. Geological Survey Scientific Investigations Map 2985, p. 48, http://www.usgs.gov/pubprod (accessed April 2020).

Samson, S.D., Hibbard, J.P., and Wortman, G.L., 1995, Nd isotopic evidence for juvenile crust in the Carolina terrane, southern Appalachians: Contributions to Mineralogy and Petrology, v. 121, p. 171–184, doi:10.1007/s004100050097.

Sayers, J., and Uddin, A., 2010, Provenance of the Cretaceous Tuscaloosa Formation in eastern Alabama and western Georgia: Geological Society of America Abstracts with Programs, v.

42, p. 72, https://gsa.confex.com/gsa/2010NE/finalprogram/abstract_170163.htm (accessed June 2019).

Scherer, E.E., Whitehouse, M.J., and Münker, C., 2007, Zircon as a monitor of crustal growth: Elements, v. 3, p. 19–24, doi:10.2113/gselements.3.1.19.

Schwarz, S.A., 2001, Secondary Ion Mass Spectroscopy, *in* Encyclopedia of Materials: Science and Technology, Elsevier, p. 8283–8290, doi:10.1016/b0-08-043152-6/01482-0.

Schwimmer, D.R., Stewart, J.D., and Williams, G.D., 1994, Giant fossil coelacanths of the late Cretaceous in the eastern United States: Geology, v. 22, p. 503–506, doi:10.1130/0091-7613(1994)022<0503:GFCOTL>2.3.CO;2.

Scwhimmer, D., 2002, King of the Crocodylians: The Paleobiology of Deinosuchus (LIfe of the Past) (James O. Farlow, Ed.): Bloomington, Indiana University Press, 240 p., doi:10.1669/0883-1351(2003)018<0080:br>2.0.co;2.

Secor, D.T., Samson, S.L., Snoke, A.W., and Palmer, A.R., 1983, Confirmation of the Carolina slate belt as an exotic terrane: Science, v. 221, p. 649–651, doi:10.1126/science.221.4611.649.

Slagstad, T., Roberts, N.M.W., and Kulakov, E., 2017, Linking orogenesis across a supercontinent; the Grenvillian and Sveconorwegian margins on Rodinia: Gondwana Research, v. 44, p. 109–115, doi:10.1016/j.gr.2016.12.007.

Society, A.G., 1968, Facies Changes in the Selma Group in Central and Eastern Alabama: Guidebook, v. 6, p. 69, internal-pdf://0237195489/ags6.pdf (accessed July 2019).

Stern, R.A., 2009, Chapter 1: An Introduction to Secondary Ion Mass Spectrometry (SIMS) in Geology, *in* Mineralogical Association of Canada Short Course 41, Toronto, p. 1–18.

Szabo, M. W., Osborne, E. W., Copeland, C. W. Jr., N.T.L., 1988, Geologic Map of Alabama,

Special Map 220, scale 1:250,000.: Geological Survey of Alabama.

Tew, B.H., and Ebersole, S., 2008, Geology of Alabama | Encyclopedia of Alabama: The Enclylopedia of Alabama, http://www.encyclopediaofalabama.org/article/h-1549 (accessed January 2020).

Tollo, R.P., Aleinikoff, J.N., Bartholomew, M.J., and Rankin, D.W., 2004, Neoproterozoic A-type granitoids of the central and southern Appalachians: Intraplate magmatism associated with episodic rifting of the Rodinian supercontinent: Precambrian Research, v. 128, p. 3–38, doi:10.1016/j.precamres.2003.08.007.

Tollo, R.P., Bartholomew, M.J., Hibbard, J.P., and Karabinos, P.M., 2010, From Rodinia to Pangea: The Lithotectonic Record of the Appalachian Region (R. P. Tollo, M. J. Bartholomew, J. P. Hibbard, & P. M. Karabinos, Eds.): Boulder, Geological Society of America, 431–454 p., doi:10.1130/mem206.

Tucker, R., 2011, U-Th Dating of zircons from a Holocene volcanic eruption (Dayingshan Volcano, Tengchong Volcanic Field): Insights into magma chamber storage: Auburn University, 88 p.

Tucker, R.T., Zou, H., Fan, Q., and Schmitt, A.K., 2013, Ion microprobe dating of zircons from active Dayingshan volcano, Tengchong, SE Tibetan Plateau: Time scales and nature of magma chamber storage: Lithos, v. 172–173, p. 214–221, doi:10.1016/j.lithos.2013.04.017.

Unrug, R., 1997, Rodinia to Gondwana: The geodynamic map of Gondwana supercontinent assembly: GSA Today, v. 7, p. 1–6, doi:10.1016/s0899-5362(97)83550-6.

Wenner, D.B., 1981, Oxygen isotopic compositions of the late orogenic granites in the Southern Piedmont of the Appalachian Mountains, U.S.A., and their relationship to subcrustal structures and lithologies: Earth and Planetary Science Letters, v. 54, p. 186–199,

doi:10.1016/0012-821X(81)90002-9.

Zhang, C. L., Ye, X. T., Zou, H.B., Chen, X. Y., 2016. Neoproterozoic sedimentary basin evolution in southwestern Tarim, NW China: New evidence from field observations, detrital zircon U-Pb ages and Hf isotope compositions. Precambrian Research, v. 280, p. 31-45.

Zou, H. B., 2007, Quantitative Geochemistry: Imperial College Press, 287 p.

Zou, H. B., Fan, Q., Schmitt, A.K., and Sui, J., 2010, U-Th dating of zircons from Holocene potassic andesites (Maanshan volcano, Tengchong, SE Tibetan Plateau) by depth profiling: Time scales and nature of magma storage: Lithos, v. 118, p. 202–210, doi:10.1016/j.lithos.2010.05.001.

Zou, H. B., Fan, Q.C., Zhang, H. F., Schmitt, A.K., 2014. U-series zircon age constraints on the plumbing system and magma residence times of the Changbai volcano, China/North Korea border. Lithos, v. 200-201, p. 169-180.

Zou, H. B., Vazquez, J., Fan, Q.C., 2020. Timescales of magmatic processes in post-collisional potassic lavas, northwestern Tibet. Lithos, v. 358-359, 105418.

APPENDICES

Appendix 1. U/Pb isotope data and ages for 19MGM-1 zircons measured by SIMS.

Age (Ma)	Age (Ma)	Age (Ma)	Age (Ma)	Age (Ma)	Age (Ma)	Degree of discordance

$^{206}Pb/^{238}U$	$^{206}Pb/^{238}U$	$^{207}Pb/^{235}U$	$^{207}Pb/^{235}U$	$^{207}Pb/^{206}Pb$	$^{207}Pb/^{206}Pb$	
	1 s.e.		1 s.e.		1 s.e.	
504	37	549	56	736	207	8.10%
329	12	323	11	283	68	-1.70%
452	18	464	19	522	66	2.50%
1857	62	1761	32	1649	26	-5.50%
1244	35	1243	22	1240	19	-0.10%
760	40	783	39	848	114	2.90%
1206	35	1215	24	1230	17	0.70%
761	29	773	28	807	89	1.50%
584	37	655	26	906	88	10.80%
381	15	364	14	263	88	-4.40%
1092	62	1139	66	1230	171	4.10%
454	16	455	16	458	54	0.10%
1385	69	1302	41	1168	48	-6.40%
1170	37	1167	25	1161	12	-0.30%
525	49	546	46	636	91	3.90%
451	19	455	16	475	32	0.90%
1185	57	1182	35	1175	23	-0.30%
1290	84	1249	51	1179	20	-3.30%
1227	50	1198	38	1147	39	-2.40%
1234	50	1251	32	1281	54	1.40%
356	17	357	14	367	49	0.40%
1198	72	1135	44	1016	32	-5.60%
1110	29	1121	19	1143	14	1.00%
1278	49	1298	33	1332	31	1.50%
419	14	430	14	491	43	2.60%
1087	49	1064	33	1017	7	-2.20%

Appendix 2. U/Pb isotope data and ages for 19CSG-1 zircons measured by SIMS.

Age (Ma) $^{206}Pb/^{238}U$	Age (Ma) $^{206}Pb/^{238}U$	Age (Ma) $^{207}Pb/^{235}U$	Age (Ma) $^{207}Pb/^{235}U$	Age (Ma) $^{207}Pb/^{206}Pb$	Age (Ma) $^{207}Pb/^{206}Pb$	Degree of discordance
	1 s.e.		1 s.e.		1 s.e.	
333	17	372	13	626	78	10.60%
989	31	1019	24	1082	36	2.90%
441	17	429	24	365	125	-2.80%
424	14	470	30	698	135	9.70%
461	15	453	12	418	30	-1.60%
449	18	455	21	484	99	1.30%
1061	36	1111	29	1211	62	4.50%
451	19	490	28	676	118	7.90%
446	20	450	23	472	124	1.00%
652	86	818	57	1302	131	20.30%
1057	42	1053	28	1045	19	-0.40%
321	10	331	11	403	46	3.10%
325	12	342	20	459	131	5.00%
1041	43	1047	29	1060	29	0.60%
992	39	984	31	968	37	-0.80%
718	66	776	63	946	70	7.40%
434	17	453	15	550	70	4.10%
317	11	329	10	417	37	3.70%
1102	43	1095	30	1079	26	-0.60%
1020	30	1031	24	1054	41	1.10%
1250	59	1294	44	1367	58	3.40%
929	23	962	19	1038	20	3.40%
462	22	490	27	624	116	5.80%

994	45	960	32	883	44	-3.50%
455	19	463	19	498	76	1.60%
1090	36	1085	29	1075	63	-0.50%
999	41	1014	33	1047	49	1.50%
875	28	913	23	1007	45	4.20%
431	19	433	17	443	79	0.40%
443	19	474	22	625	84	6.50%
1287	50	1307	38	1340	29	1.50%
446	12	449	11	465	29	0.70%
299	7	313	11	419	73	4.50%
320	9	328	10	388	71	2.60%
448	12	445	17	428	67	-0.70%
1150	34	1217	48	1338	117	5.50%
1038	28	1074	21	1148	23	3.40%
692	28	735	26	870	39	5.90%
331	9	338	13	387	83	2.10%
1191	44	1210	32	1243	23	1.60%